

The Sokoban Random Walk: A Trapping Perspective

Prashant Singh,^{1,*} Eli Barkai,^{1,2} and David A. Kessler¹

¹*Department of Physics, Bar-Ilan University, Ramat Gan 52900, Israel*

²*Institute of Nanotechnology and Advanced Materials, Bar-Ilan University, Ramat Gan 52900, Israel*

We study caging/trapping in Sokoban-type models, featuring a random walker moving through a disordered medium of obstacles and capable of pushing some obstacles blocking its path. In one-dimension, we allow the walker to push up to an arbitrary N_P number of obstacles. For $N_P \gg 1$, we use large-deviation theory to show that the survival probability to remain uncaged exhibits crossover from an exponential decay with time at intermediate times to a stretched-exponential decay at long times, with an exponent $1/3$ independent of N_P . The long-time exponent matches the Balagurov–Vaks–Donsker–Varadhan (BVDV) theory of the classical trapping problem, while the exponential decay is qualitatively distinct from the Rosenstock’s intermediate-time theory for classical trapping. Similarly, in two dimensions, numerical simulations reveal that both the Sokoban model and its generalized version exhibit long-time stretched-exponential relaxation with exponent $1/2$, again consistent with the BVDV theory. Finally, in two dimensions, we find that the mean trap size is nonmonotonic in ρ : it is small at both low and high densities, but reaches a peak at a characteristic density ρ_* . We estimate $\rho_* \approx 0.55$ for the Sokoban model and $\rho_* \approx 0.675$ for the generalized Sokoban model.

I. INTRODUCTION

Transport in a disordered medium is a classic problem in statistical physics that has been extensively studied in the context of various physical systems, such as percolation [1–3], charge transport [4, 5], motion in the porous medium [6], diffusion of single molecules in the cell environment [7, 8] and active models in complex environment [9, 10]. A commonly studied model in percolation is the de Gennes’ *ant in a labyrinth* model [11]; see also [2, 3] for reviews. In this model, a discrete-time random walker moves in a two-dimensional disordered lattice with randomly placed fixed obstacles, and in every move, it can jump with equal probability to one of its neighboring sites, provided that the target site does not contain an obstacle. The obstacles themselves are initially randomly distributed with some fixed density ρ (where $0 \leq \rho \leq 1$).

The ant in a labyrinth model (henceforth referred to as AIL) exhibits a percolation transition at the critical density ρ_c : for $\rho \leq \rho_c$, the walker can escape to infinity while for $\rho > \rho_c$, the escape is not possible. The value of ρ_c itself depends on the dimensionality as well as on the lattice type. For example, $\rho_c \approx 0.407$ in a two-dimensional square lattice [12, 13].

Interestingly, recent studies by Reuveni and coworkers reveal that allowing the walker to even minimally modify its local environment leads to the loss of the percolation transition in two dimensions [14, 15]. These studies introduced a new type of random walk, named *Sokoban*, the model having been inspired by a video game created by Hiroyuki Imabayashi in 1981 [16]. The Sokoban walker, unlike an AIL walker, has the ability to push some of the obstacles that block its way. This pushing ability, however, is limited in the sense that the walker

can displace only a finite number of obstacles (explained precisely later). On physical grounds, such a finiteness can naturally arise whenever the obstacles are smaller than or comparable in size to the random walker, such as in experiment involving bristle robot moving in an arena of movable obstacles [17] or energized active particle pushing the surrounding particles [18, 19]. The loss of percolation for the Sokoban model clearly signals a fundamental difference between the scenarios where the environment is fixed versus those where it can be shaped to small extent by the walker.

Although the percolation transition is lost in the two-dimensional Sokoban model, we showed in a recent Letter that it exhibits a dynamical crossover in the underlying trapping mechanisms [20]. Here, “trapping” means that the walker becomes caged to a finite, closed domain, thereby suppressing long-range transport (explained precisely later). At high obstacle density, traps are essentially predetermined by the initial obstacle configuration, whereas at low density a self-trapping mechanism emerges in which the Sokoban dynamically generates its own trap. To characterize these mechanisms, we examine the following observables: (i) the disorder-averaged survival probability that the walker remains uncaged/untrapped until time n , (ii) the average trapping time $\langle n_T \rangle$ and, (iii) the probability of trap sizes and its average $\langle A_T \rangle$. Here $\langle n_T \rangle$ and $\langle A_T \rangle$ denote averages over the disorder realizations as well as the walker’s stochastic dynamics.

The purpose of this paper is to investigate the trapping aspects of the Sokoban random walk in greater detail. We also study the variants of the model in order to test the universality of the emergent trapping features. To this end, we introduce the one-dimensional N_P -Sokoban model, in which the walker can push up to an arbitrary N_P (≥ 0) number of obstacles; $N_P = 1$ corresponds to the model of Reuveni and coworkers. For $N_P \gg 1$, a large-deviation analysis reveals that the Sokoban model be-

* prashantsinghramitay@gmail.com

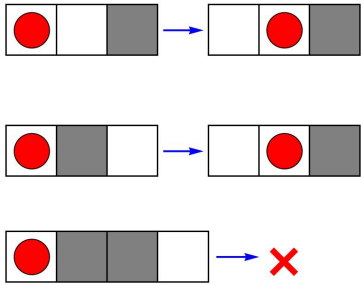


FIG. 1. The dynamical rules governing the time evolution of a N_P -Sokoban walker with $N_P = 1$. The walker is shown in red, obstacles in gray, and vacant sites in white. As shown in the top panel, a jump to a nearest-neighbor site is allowed if the target site is vacant. If the target site is occupied, the walker can still move by pushing the obstacle to the next-nearest site, provided that this site is vacant; see the middle panel. If this condition is not satisfied, as shown in the bottom panel, the attempted jump is unsuccessful.

longs to the Balagurov-Vaks-Donsker-Varadhan (BVDV) universality class for the classical trapping problem (see Eq. (1) later) [2, 3]. In other words, the disorder-averaged survival probability to remain uncaged exhibits a stretched-exponential decay at late times, with stretch exponent $1/3$ that is independent of N_P .

In two dimensions, we perform numerical simulations of the Sokoban model and a generalized variant (introduced in Sec. II), and find long-time stretched-exponential relaxation for the survival probability, with exponent $1/2$ again consistent with the BVDV theory. At the same time, the Sokoban model displays notable differences from the classical trapping problem: (i) modified prefactors accompanying the stretched-exponential decay, (ii) a distinct intermediate-time regime that deviates from the Rosenstock approximation for classical trapping (see Eq. (2)), and (iii) geometry of the created trap in two-dimensions which bears signature of the dynamical crossover between the two trapping mechanisms discussed above.

The rest of our paper is structured as follows: Sec. II introduces the models, defines precisely the observables of interest, and announces the main results of our paper. In Sec. III, we will use a renewal framework to derive the statistics of the trapping time and trap size for the N_P -Sokoban model for a given initial obstacle configuration. We then perform the disorder-averaging of these results in Sec. IV to calculate the survival probability. Building on the insights gained from these sections, we study the two-dimensional Sokoban model and its variant in Sec. V using numerical simulations. This is then followed by our conclusions and open directions in Sec. VI.

II. MODEL, PRELIMINARIES AND SUMMARY OF THE RESULTS

We first describe the Sokoban model introduced by Reuveni and co-workers [14]. Consider a square d -dimensional lattice system of size \mathcal{N}^d , where initially every site can accommodate an obstacle with probability ρ and remain vacant with the complementary probability $(1 - \rho)$. Taking \mathcal{N} to be odd, we place our discrete-time random walker initially at the center and consider the limit $\mathcal{N} \rightarrow \infty$. In every move, the walker chooses one of its z_d neighboring sites with an equal probability $1/z_d$ and attempts a jump to that site. One has $z_d = 2$ in one dimension, $z_d = 4$ in two dimensions, and so on.

The jump is successful if the target site is vacant; see top panel in Fig. 1 for the one-dimensional case. On the other hand, if the target site is occupied by an obstacle, the walker can still move one step by pushing the obstacle in the same direction. The pushing is allowed provided the next site beyond the obstacle is vacant; see the middle panel in the figure. If this condition is met, both the walker and the obstacle move one step in that direction. Otherwise, they do not move, as shown in the bottom panel. Hence, the Sokoban walker is capable of pushing the obstacles and it can at most push one obstacle in a given move. In this paper, we focus on $d = 1, 2$.

To test the universality of the trapping phenomenon, we also analyze variants of the Sokoban model with pushing rules modified relative to the one described above. As pointed out before, in one dimension, we consider the most general case where the Sokoban is capable of pushing up to an arbitrary N_P number of obstacles (“P” for “pushing”). We will refer to this model as the N_P -Sokoban walk.

We also mentioned above a generalized two-dimensional variant of the Sokoban dynamics. In this extension, the obstacle can be pushed to any of its three neighbouring sites (except the site containing the walker) with equal probability $1/3$, provided that this target site is vacant. This is different than the two-dimensional Sokoban model introduced before, where the obstacle can be pushed only in the direction of the walker’s attempted motion. We will refer to this variant as the G-Sokoban walk (“G” for “generalized”). Our aim is to investigate whether the properties of the Sokoban model are model-specific or if they are common to other models with different pushing capabilities.

A. Reactive trapping: a brief survey of known results

Before we proceed with our analysis, it is important to precisely explain what we mean by trapping. In the literature, a commonly studied form of trapping is reactive trapping [21–24]. To understand it, consider a random walker moving through a medium of randomly placed

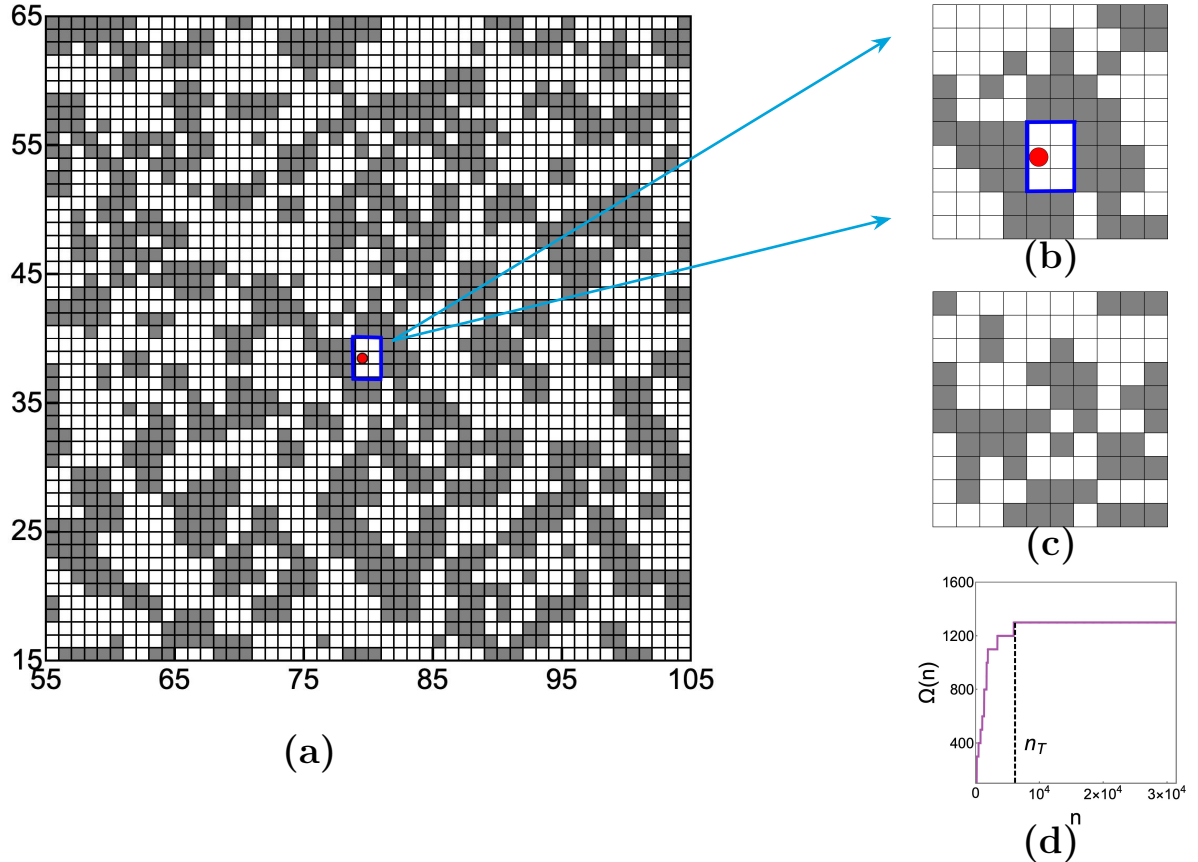


FIG. 2. Trapping by caging of a Sokoban walker in two dimensions, starting from the origin. Panel (a) displays the final configuration in a 50×50 window, covering the ranges 55–105 along the x -axis and 15–65 along the y -axis, from a representative realization at $\rho = 0.4$. The Sokoban walker (shown in red) is trapped inside a cage (shown in blue) formed by surrounding obstacles (shown in gray), and its position in the figure is (80, 40) (the walker initially is at the origin, outside the displayed window). Panel (b) shows a magnified view of a part of the configuration responsible for trapping, with the trap size $A_T = 6$. In panel (c), we show the same part at the initial time and see that the trap does not exist initially. The Sokoban walker at some later time enters this region and modifies it into a trap in panel (b) through successive interaction with the obstacles. Finally, in panel (d), we have plotted the number of distinct visited sites, $\Omega(n)$, as a function of time n . This number is saturated for all $n \geq n_T$ with $n_T = 6 \times 10^3$.

obstacles and it is trapped immediately upon encountering an obstacle. The dynamics is terminated upon first encounter with an obstacle, and this mimics a perfect reaction center trapping the walker.

In reactive trapping, the walker does not reshape its environment, and at first sight this setting may appear very different from the Sokoban model. However, the Sokoban model shares striking similarities with reactive trapping, while also exhibiting important differences that we analyze in later sections. For this reason, we briefly survey the relevant results for the reactive trapping problem.

A widely studied quantity in this context is the survival probability $\phi(n)$ that the walker has not yet encountered any obstacle up to some time n [2, 3]. Balagurov and Vaks [22] and Donsker and Varadhan [23] proved that this survival probability decays in the long-time limit, in

d dimensions, as

$$\phi(n) \sim \exp\left(-\beta_d \lambda^{\frac{2}{d+2}} n^{\frac{d}{d+2}}\right), \quad \text{with } n \lambda^{2/d} \gg 1, \quad (1)$$

with $\lambda = |\ln(1 - \rho)|$ and $\beta_1 = 3\pi^{2/3}/2$ and $\beta_2 \approx 3.4$ in one and two dimensions [23, 25]. We refer to Eq. (1) as the Balagurov-Vaks-Donsker-Varadhan (BVDV) theory, and it characterizes the asymptotic decay of the reactive-trapping-based survival probability at late times.

At intermediate times, an approximation due to Rosenstock [21, 24] works well, especially at small densities:

$$1 - \phi(n) \sim \begin{cases} \sqrt{n\rho^2}, & \text{in 1d,} \\ n\rho/\log n & \text{in 2d.} \end{cases} \quad (2)$$

One of our main findings is that the Sokoban model and its variants in one and two dimensions fall into the same universality class as reactive trapping, but with important differences that we demonstrate later.

B. Trapping by caging

We now introduce cage-trapping, the process which will describe the Sokoban model. Here, trapping is induced by physical rearrangements of the environment, rather than by perfect chemical reaction between the walker and the obstacle. To characterize this form, we look at the number of distinct lattice sites $\Omega(n)$ visited by the Sokoban walker [26–28]. For a given initial configuration of obstacles, $\Omega(n)$ is a nondecreasing function of n , and at each step it can either increase by one or remain unchanged. It saturates only when the walker becomes caged from all directions by the obstacles. Otherwise, it continues to grow indefinitely. In Fig. 2(a,b,c), we show a schematic of the final configuration in which the walker has been caged, and panel (d) of the same figure shows the saturation of $\Omega(n)$. Therefore, by monitoring whether $\Omega(n)$ has saturated or not, we can say whether the walker is cage-trapped or not for that trajectory.

In this paper, we focus mainly on this trapping by caging and we will, for simplicity, refer to this form as the trapping phenomenon. Consider now the trapped scenario, i.e., $\Omega(n)$ has saturated to a finite value for a given initial configuration and a given realization of the walker's stochastic dynamics. Let n_T be the time when $\Omega(n)$ attains its saturation value for the first time. This is the time when the walker completes its exploration of new distinct sites and it is clearly a random quantity. We will refer to n_T as the trapping time. Averaging it over initial obstacle configurations and the walker's stochastic dynamics, we obtain the average $\langle n_T \rangle$.

To infer trapping by caging, we have to monitor $\Omega(n \rightarrow \infty)$. However, in simulations, we cannot evolve the system for an infinite time and we therefore introduce a simulation stopping time τ_{sim} , which sets the duration for which we run each realization. In our work, we choose $\tau_{\text{sim}} \sim 10^8$. Operationally, for each realization we record the final value $\Omega(\tau_{\text{sim}})$ and then scan the trajectory backward to identify the earliest time n_T such that $\Omega(n_T) = \Omega(\tau_{\text{sim}})$. For obstacle densities considered in this work, the chosen value of the simulation time is at least $\tau_{\text{sim}} \sim 100\langle n_T \rangle$. This ensures that $\Omega(n)$ has reached its final value well before τ_{sim} and remains unchanged at least over a time window $100\langle n_T \rangle$. Importantly, since the value of $\Omega(n)$ may only increase by one at each move, its saturation in the given time window can be detected unambiguously for each realization; see Fig. 2(d). Further details on the numerical simulations is provided in Appendix A.

Apart from the trapping time, we are also interested in the trap size A_T , the number of vacant sites inside the trap. Once again, we have schematically illustrated A_T in Fig. 2 and the procedure of generating it in numerical simulations is provided in Appendix A. Averaging the trap size over initial obstacle configurations and the walker's stochastic dynamics, we obtain the average $\langle A_T \rangle$.

In addition, averaging over the same ensemble, we will

also study the probability that $\Omega(n)$ has not attained its saturation value till time n . Physically, this represents the disorder-averaged survival probability $S(n)$ that the walker has not been caged up to time n . This is different from $\phi(n)$ introduced before in the reactive-trapping context. Remember that $\phi(n)$ depends only on the walker's first encounter with an obstacle. On the other hand, $S(n)$ depends on the walker's interaction with multiple obstacles. We study $S(n)$, $\langle n_T \rangle$ and $\langle A_T \rangle$ for the Sokoban model and its variants introduced above. Let us now summarize the main results of our paper.

C. Summary of results

- *Stretched-exponential relaxation:* We show that the survival probability, $S(n)$, exhibits a stretched-exponential decay at late times

$$S(n) \sim \exp[-f_d(\rho)n^{\mu_d}], \quad (3)$$

with exponents $\mu_1 = 1/3$ and $\mu_2 = 1/2$ in one and two dimensions, respectively. We analytically prove that $f_1(\rho) = 3\pi^{\frac{2}{3}}|\ln(1-\rho)|^{\frac{2}{3}}/2^{\frac{5}{3}}$ in one dimension. In two dimensions, we use numerical simulations to demonstrate Eq. (3) and extract an estimate of $f_2(\rho)$. Interestingly, both μ_1 and μ_2 exponents match with the BVDV formula in Eq. (1).

- *Moderate-time behavior:* Eq. (3) captures the long-time behavior of $S(n)$. For small to moderate values of n , we show

$$1 - S(n) \sim \begin{cases} n^2\rho^4 & \text{for 1d Sokoban,} \\ n^{\epsilon(\rho)}, & \text{for 2d Sokoban,} \end{cases} \quad (4)$$

where the exponent $\epsilon(\rho)$ depends on the density. This behavior is qualitatively different from the moderate-time Rosenstock approximation for $\phi(n)$ in Eq. (2). This highlights how, despite similarities in long-time scaling, the short to moderate time dynamics of the two survival probabilities, $\phi(n)$ and $S(n)$, are completely different.

- *Generalized Sokoban models:* For the N_P -Sokoban model, we prove that the survival probability $S(n)$ has a large-deviation form in the joint limit $n \gg 1$ and $N_P \gg 1$ while keeping the ratio $\omega = n/(N_P)^3$ fixed

$$\lim_{\substack{N_P \gg 1, n \gg 1 \\ \omega = n/(N_P)^3 \text{ fixed}}} \frac{-\ln S(n)}{N_P} = \mathcal{I}(\omega). \quad (5)$$

The corresponding rate function $\mathcal{I}(\omega)$ is given by Eqs. (52) and (53). It has the asymptotic behaviors

$$\mathcal{I}(\omega) \simeq \begin{cases} \frac{\pi^2\rho^2}{32(1-\rho)^2}\omega, & \text{for } \omega \rightarrow 0, \\ \frac{3\pi^{2/3}\lambda^{2/3}}{2^{5/3}}\omega^{1/3} & \text{for } \omega \rightarrow \infty, \end{cases} \quad (6)$$

implying that the survival probability changes from an exponential decay at $n \ll (N_P)^3$ to the same 1/3-stretched-exponential decay as in Eq. (3) at $n \gg (N_P)^3$. Thus, the long-time stretched-exponential decay of $S(n)$ is completely universal, independent of N_P .

For the two-dimensional G-Sokoban model, the survival probability, $S(n)$, is also characterized by the exponent $\mu_2 = 1/2$, same as in Eq. (3). Thus, modifying the microscopic pushing rules does not qualitatively alter the long-time stretched-exponential exponent even in two dimensions.

- *Emergence of a trapping crossover:* For the two-dimensional Sokoban model, our simulations also suggest that the percolation transition is lost [14]. However, our study goes further to reveal that the Sokoban model nonetheless exhibits a dynamical crossover in the underlying trapping mechanisms. We characterize the crossover in terms of the average trap size $\langle A_T \rangle$ being a nonmonotonic function of the obstacle density ρ : $\langle A_T \rangle$ initially increases as ρ decreases, reaches a maximum at ρ_* , and then diminishes below this threshold; see Fig. 11 later. For $\rho > \rho_*$, trapping is dominated by pre-existing cages in the initial obstacle configuration, whereas for $\rho < \rho_*$ it is dominated by self-created cages generated dynamically by the walker through interactions with obstacles; also see Fig. 2(b,c). Using numerical simulations, we estimate $\rho_* \approx 0.55$ for the Sokoban model and $\rho_* \approx 0.675$ for the G-Sokoban model.

In what follows, we will derive all of the above results analytically in one dimensions. Building on the insights gained, we will then look at the two-dimensional models using extensive numerical simulations.

III. N_P -SOKOBAN MODEL IN ONE DIMENSION

For the Sokoban walker moving in one dimension (say x axis) and placed initially at the origin, the total space available for the motion, for a fixed *initial* obstacle configuration, is determined by the number of obstacles it can push. For every initial realization of obstacle positions, the walker can push up to N_P obstacles on the positive x -axis and up to N_P obstacles on the negative x -axis. In each direction ($+x$ or $-x$), the obstacles can be pushed up to the point where the first $(N_P + 1)$ obstacles in that direction are situated on consecutive sites. Beyond this point, the walker cannot push obstacles further in that direction for that particular realization. For illustration, Fig. 3 shows the case $N_P = 2$. Panel (a) shows the configuration at the initial time with walker at the origin. Panel (b) shows the configuration at a later time where obstacles have been maximally pushed and cannot

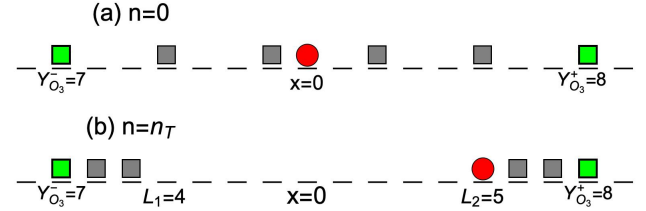


FIG. 3. Schematics of the one-dimensional N_P -Sokoban model with $N_P = 2$. Panel (a) shows a realization of the walker and obstacles at the initial time. The walker, located at the origin, is shown in red and obstacles are shown in gray and green. They are identical, but distinguished here to illustrate that the gray ones will be pushed by the walker. As time evolves, the gray obstacles on both sides of the origin are pushed until time $n = n_T$ in panel (b). Here, the pushed (gray) obstacles on each side lie on consecutive sites in front of the green obstacle. Beyond this point, the walker cannot push the obstacles due to its finite ($N_P = 2$) pushing capacity. Consequently, in every realization, the Sokoban walker is confined inside a finite interval $[-L_1, L_2]$ throughout its time evolution with L_1 and L_2 determined by the positions of the $(N_P + 1)$ -th obstacles on the $x < 0$ and $x > 0$ sides, respectively, see Eq. (7). These obstacles are shown in green in this figure. For the chosen realization in this figure, we have $L_1 = 4$ and $L_2 = 5$ determined by the positions of the green obstacles, $-Y_{O_3}^- = -7$ and $Y_{O_3}^+ = 8$, in either direction using Eq. (7).

be pushed further. At this point, the first three obstacles in both $+x$ and $-x$ directions are located on consecutive sites. In the figure, observe that the third obstacle on each side (shown in green) remains fixed throughout the evolution.

Likewise, for general N_P , in each direction the $(N_P + 1)$ -th obstacle remains immobile, while only the first N_P obstacles can be pushed until the first $(N_P + 1)$ obstacles in that direction occupy consecutive sites, as mentioned before. For a given initial realization of obstacle configuration, we denote the position of the $(N_P + 1)$ -th obstacle in the $-x$ direction by $-Y_{O_{N_P+1}}^-$, and the position of the $(N_P + 1)$ -th obstacle in the $+x$ direction by $Y_{O_{N_P+1}}^+$. Then, in this realization the walker is confined inside the interval $[-L_1, L_2]$ throughout its evolution such that

$$L_1 = \left(Y_{O_{N_P+1}}^- - N_P - 1 \right), \quad L_2 = \left(Y_{O_{N_P+1}}^+ - N_P - 1 \right). \quad (7)$$

and reflecting conditions at the two ends; also see Fig. 3. Since the obstacles are initially distributed randomly, both L_1 and L_2 are also random quantities. Nonetheless, they are bounded from below as $L_1 \geq 0$, $L_2 \geq 0$. The idea now is to fix the values of L_1 and L_2 and derive the survival probability, trap size, and trapping time conditioned on these values. These conditional quantities will then be averaged over the probabilities of L_1 and L_2 to obtain the disorder-averaged observables.

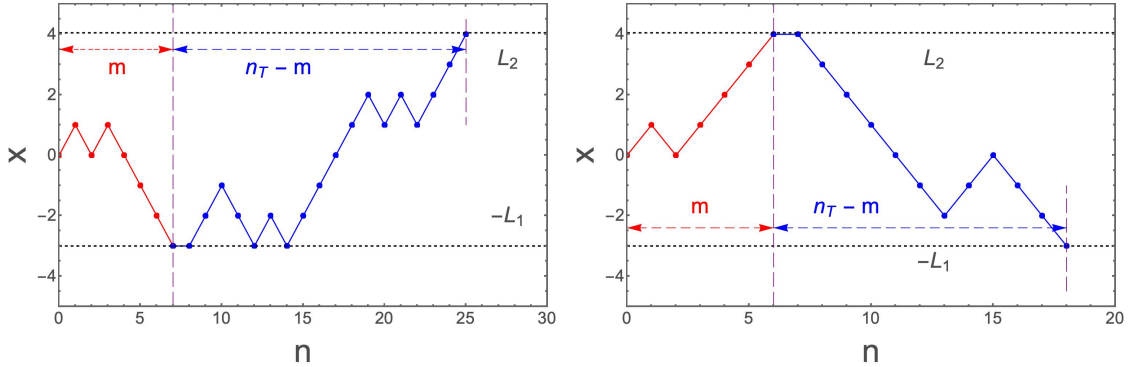


FIG. 4. *Left Panel:* A schematic illustration of the trajectory of the random walker, where it reaches $x = -L_1$ at the m -th time step and subsequently reaches $x = L_2$ at a later time step n_T . For the shown trajectory, $L_1 = 3$, $L_2 = 4$, $m = 7$ and $n_T = 25$. We have broken the trajectory in two parts: from 0 to m shown in red and from m to n_T shown in blue. *Right Panel:* Here we have shown an example of the second type of trajectories where the walker first reaches $x = L_2$ at the m -th time step and then reaches $x = -L_1$ at n_T time step. For this trajectory, $L_1 = 3$, $L_2 = 4$, $m = 6$ and $n_T = 18$.

A. Conditional survival dynamics for fixed L_1 and L_2

For given L_1 and L_2 , the walker will be trapped when the number of distinct sites it has visited saturates and no longer increases with time. As illustrated in Fig. 3(b), this will happen whenever the walker has visited both the boundary sites, $-L_1$ and L_2 , at least once. Let n_T be the first time it hits one of the interval boundaries given that it has previously hit the other one at least once. We denote this probability by $P(n_T|L_1, L_2)$ for given values of L_1 and L_2 . As mentioned before, our eventual goal in this section is to calculate the disorder-averaged probability $\langle P(n_T|L_1, L_2) \rangle_{L_1, L_2}$. Throughout this section, we will use the notation $\langle \dots \rangle_{L_1, L_2}$ to denote the expectation value with respect to the probabilities of L_1 and L_2 .

To proceed, we will calculate various terms that contribute to $P(n_T|L_1, L_2)$. We begin by considering the simplest scenario where $L_1 = 0$, $L_2 = 0$ (or equivalently $L = (L_1 + L_2) = 0$). In this case, the walker is immediately trapped at its initial position. Consequently, one has

$$P(n_T|L_1 = 0, L_2 = 0) = \delta_{n_T, 0}. \quad (8)$$

Here $\delta_{n_T, 0}$ stands for the Kronecker delta. Next, we consider the other case when $L \neq 0$, *i.e.*, at least one of L_1 or L_2 is non-zero. Two possible scenarios can occur. The first is when the walker hits $x = -L_1$ first at least once and then reaches $x = L_2$ at some later time n_T , see the left panel in Fig. 4. The second scenario is the complementary one, where the walker first reaches $x = L_2$ and then hits $x = -L_1$ at time n_T , see the right panel in the same figure. We begin with the first case and denote by m the first time the walker reaches $x = -L_1$. As shown in the left panel, we now divide the whole trajectory into two parts: (i) the $[0, m]$ part shown in red and (ii) the $[m, n_T]$ part shown in blue. In the red part, the walker starts from the origin and makes

its first visit to $-L_1$ at time m but with the constraint that it has not reached L_2 before. Thus the statistical weight of this part is equal to the first-passage probability $\mathcal{F}_1(m|x_0 = 0, \{x_j\}_{j=1}^{m-1} < L_2)$ to $-L_1$ such that the positions x_1, x_2, \dots, x_{m-1} of the random walk at all intermediate times are smaller than L_2 . For the blue part, the walker starts at $x_0 = -L_1$ and reaches L_2 for the first time in the remaining time interval $(n_T - m)$, see Fig. 4 (left panel). Hence, the statistical weight of this segment is equal to the first-passage probability $\mathcal{F}_2(n_T - m|x_0 = -L_1)$ to L_2 without any constraint at intermediate times.

One can now express the conditional probability of observing a trapping time n_T for this class of trajectories as

$$P_{C_1}(n_T|L_1, L_2) = \sum_{m=0}^{n_T} \mathcal{F}_1(m|x_0 = 0, \{x_j\}_{j=1}^{m-1} < L_2) \times \mathcal{F}_2(n_T - m|x_0 = -L_1). \quad (9)$$

Here the subscript ‘ C_1 ’ in $P_{C_1}(n_T|L_1, L_2)$ is used to indicate that we are looking at the probability conditioned on the fact that the walker first hits $x = -L_1$ and then reaches $x = L_2$ at some later time. Moreover, we have utilized the property that the two segments (red and blue) of the trajectory are statistically independent, allowing us to write the total probability as a sum of the product of the individual weights from the two segments.

We next consider the other case, in which the walker hits $x = L_2$ first and then reaches $x = -L_1$ at some later time. As shown in the right panel of Fig. 4, one can again apply the same reasoning as before, dividing the trajectory into two segments and calculating the weights from each. The conditional probability from this class of trajectories is then given by

$$P_{C_2}(n_T|L_1, L_2) = \sum_{m=0}^{n_T} \mathcal{F}_2(m|x_0 = 0, \{x_j\}_{j=1}^{m-1} > -L_1) \times \mathcal{F}_1(n_T - m|x_0 = L_2), \quad (10)$$

where ‘ \mathcal{C}_2 ’, as before, emphasizes the conditional nature of the probability. Summing Eqs. (8-10), we obtain the total probability $P(n_T|L_1, L_2)$ as

$$\begin{aligned} P(n_T|L_1, L_2) &= \delta_{n_T,0}\delta_{L,0} + \sum_{m=0}^{n_T} \left[\mathcal{F}_2(n_T - m|x_0 = -L_1) \right. \\ &\times \mathcal{F}_1\left(m|x_0 = 0, \{x_j\}_{j=1}^{m-1} < L_2\right) + \mathcal{F}_1(n_T - m|x_0 = L_2) \\ &\left. \times \mathcal{F}_2\left(m|x_0 = 0, \{x_j\}_{j=1}^{m-1} > -L_1\right) \right] \Theta(L). \end{aligned} \quad (11)$$

Here $\Theta(z)$ stands for the Heaviside theta function, which

$$\mathcal{F}_1\left(m|x_0 = 0, \{x_j\}_{j=1}^{m-1} < L_2\right) = \frac{\Theta(m)\Theta(L_1)}{L} \sum_{\theta=1}^L \cos^{m-1}\left(\frac{\pi\theta}{L}\right) \sin\left(\frac{\pi\theta L_1}{L}\right) \sin\left(\frac{\pi\theta}{L}\right) + \delta_{L_1,0}\delta_{m,0}, \quad (12)$$

$$\mathcal{F}_2\left(m|x_0 = 0, \{x_j\}_{j=1}^{m-1} > -L_1\right) = \frac{\Theta(m)\Theta(L_2)}{L} \sum_{\theta=1}^L \cos^{m-1}\left(\frac{\pi\theta}{L}\right) \sin\left(\frac{\pi\theta L_2}{L}\right) \sin\left(\frac{\pi\theta}{L}\right) + \delta_{L_2,0}\delta_{m,0}, \quad (13)$$

$$\mathcal{F}_2(m|x_0 = -L_1) = \frac{\Theta(m)\Theta(L)}{\left(L + \frac{1}{2}\right)} \sum_{\theta=0}^L (-1)^\theta \cos^{m-1}\left(\frac{\pi(2\theta+1)}{2\left(L + \frac{1}{2}\right)}\right) \cos\left(\frac{\pi(2\theta+1)}{4\left(L + \frac{1}{2}\right)}\right) \sin\left(\frac{\pi(2\theta+1)}{2\left(L + \frac{1}{2}\right)}\right), \quad (14)$$

with $L = (L_1 + L_2)$. Also, by symmetry $\mathcal{F}_2(m|x_0 = -L_1) = \mathcal{F}_1(m|x_0 = L_2)$. Plugging these expressions in Eq. (11), we obtain the exact form of the trapping time probability $P(n_T|L_1, L_2)$. To check that this probability is correctly normalized, we first sum Eq. (11) over all possible values of n_T as

$$\begin{aligned} \sum_{n_T=0}^{\infty} P(n_T|L_1, L_2) &= \delta_{L,0} + \Theta(L) \sum_{m=0}^{\infty} \mathcal{F}_1\left(m|x_0 = 0, \{x_j\}_{j=1}^{m-1} < L_2\right) \sum_{n=0}^{\infty} \mathcal{F}_2(n|x_0 = -L_1) \\ &+ \Theta(L) \sum_{m=0}^{\infty} \mathcal{F}_2\left(m|x_0 = 0, \{x_j\}_{j=1}^{m-1} > -L_1\right) \sum_{n=0}^{\infty} \mathcal{F}_1(n|x_0 = L_2). \end{aligned}$$

We now use the expressions in Eqs. (12-14) to yield

$$\begin{aligned} \sum_{m=0}^{\infty} \mathcal{F}_1\left(m|x_0 = 0, \{x_j\}_{j=1}^{m-1} < L_2\right) &= \frac{L_2}{L}, \quad \sum_{m=0}^{\infty} \mathcal{F}_2\left(m|x_0 = 0, \{x_j\}_{j=1}^{m-1} > -L_1\right) = \frac{L_1}{L}, \\ \sum_{m=0}^{\infty} \mathcal{F}_2(m|x_0 = -L_1) &= \sum_{m=0}^{\infty} \mathcal{F}_1(m|x_0 = L_2) = 1. \end{aligned} \quad (15)$$

The proof of these relations is relegated to Appendices B, C. Using them, it now follows

$$\sum_{n_T=0}^{\infty} P(n_T|L_1, L_2) = 1. \quad (16)$$

Thus, our theoretical expression in Eq. (11) for the trapping time probability for fixed L_1 and L_2 is correctly normalized. Having obtained this probability, we can now look at the conditional survival probability that the Sokoban walker has not been trapped till time n

$$Q(n|L_1, L_2) = 1 - \sum_{n_T=1}^n P(n_T|L_1, L_2). \quad (17)$$

takes the value 1 if $z > 0$ and 0 otherwise. Eq. (11) indicates that the problem of finding the trapping time probability has now been reduced to calculating various first-passage probabilities. For the random walk model, it turns out to be possible to calculate these probabilities exactly, and the details of this calculation are provided in Appendices B, C. Their final expressions read as

Given that we have an exact expression for $P(n_T|L_1, L_2)$, it follows that $Q(n|L_1, L_2)$ is also exactly known. One can now utilize this exact expression to derive various asymptotic behaviors of $Q(n|L_1, L_2)$. In particular, we analyze $Q(n|L_1, L_2)$ in the joint limit of large n and large L . The intuition behind this limit is that the walker can avoid being trapped over a long time interval only if the spatial region over which it moves is also large. This leads us to consider the diffusive scaling where both n and L are large but the ratio n/L^2 is finite. We show in Appendix D that one obtains different expressions depending on whether the scaled variable n/L^2 is large or small. For

the case of large n/L^2 , we find

$$Q(n|L_1, L_2) \simeq \frac{4}{\pi} \left[\sin\left(\frac{\pi L_1}{2L}\right) + \sin\left(\frac{\pi L_2}{2L}\right) \right] \exp\left(-\frac{\pi^2 n}{8L^2}\right), \quad (18)$$

while for small n/L^2 , we get

$$Q(n|L_1, L_2) \simeq 1 - 2 \left[\operatorname{erfc}\left(\frac{L_1 + 2L_2}{\sqrt{2n}}\right) + \operatorname{erfc}\left(\frac{2L_1 + L_2}{\sqrt{2n}}\right) \right], \quad (19)$$

where $\operatorname{erfc}(z)$ represents the complementary error function. Eqs. (18-19) give the survival probabilities conditioned on the fixed values of L_1 and L_2 .

Let us next turn to the conditional trap size and trapping time. Recall that we define trap size A_T as the number of vacant sites available for the walker to move when it is trapped. As seen in Fig. 3(b), this will be equal to

$$A_T(L_1, L_2) = (L_1 + L_2 + 1). \quad (20)$$

On the other hand, due to the stochastic motion of the walker, the trapping time, $n_T(L_1, L_2)$ can take any integer value. In Appendix D, we show that the conditional average $\langle n_T | L_1, L_2 \rangle$ for both $L_1, L_2 \gg 1$ is given by

$$\langle n_T | L_1, L_2 \rangle \simeq L_1^2 + L_2^2 + 3L_1 L_2. \quad (21)$$

As expected for a diffusive process, the mean time exhibits a quadratic dependence on L_1 and L_2 , with an additional term that is linear in the product $L_1 L_2$. This expression, as shown later, will be useful for small densities of obstacles. Contrarily, for high-density values, the leading behavior will be described by L_1 and L_2 of unit order and here, we get

$$\langle n_T | L_1, L_2 \rangle \simeq 2(\delta_{L_1,0}\delta_{L_2,1} + \delta_{L_1,1}\delta_{L_2,0}). \quad (22)$$

Once again we emphasize Eqs. (20-22) are all derived for fixed L_1 and L_2 .

B. Averaging over disorder

Let us now derive the probabilities of L_1 and L_2 , which according to Eq. (7) are related to the positions of the $(N_P + 1)$ -th obstacles on the positive and negative x -axes. For simplicity, we focus on the positive x -axis, where the position of this obstacle recall is denoted by $Y_{O_{N_P+1}}^+$. Observe that starting from the lattice site $x = 1$ to $x = Y_{O_{N_P+1}}^+$, there are a total of $(N_P + 1)$ sites with obstacles while the remaining $(Y_{O_{N_P+1}}^+ - N_P - 1)$ sites are free of obstacles (see Fig. 3). Combining these two contributions, the total probability of observing $Y_{O_{N_P+1}}^+ = y$ is given by

$$q(y) = \rho^{N_P+1} (1 - \rho)^{y - N_P - 1} \frac{(y - 1)!}{N_P! (y - 1 - N_P)!}, \quad (23)$$

where y can take possible integer values satisfying $y \geq (N_P + 1)$. In the expression, the factor $(y - 1)!/N_P! (y - 1 - N_P)!$ counts the number of distinct ways in which the first N_P obstacles can be placed anywhere from $x = 1$ to $x = (y - 1)$; all these arrangements lead to the same value $Y_{O_{N_P+1}}^+ = y$.

Now using Eq. (7), we can write the probability of L_2 as

$$q(L_2|N_P) = \rho^{N_P+1} (1 - \rho)^{L_2} \frac{(L_2 + N_P)!}{N_P! L_2!}, \quad (24)$$

where $L_2 = 0, 1, 2, \dots$. Similarly for L_1 , we obtain

$$q(L_1|N_P) = \rho^{N_P+1} (1 - \rho)^{L_1} \frac{(L_1 + N_P)!}{N_P! L_1!}. \quad (25)$$

As is clear from Eq. (7), the statistics of L_1 and L_2 depend on the number of obstacles the Sokoban walker is able to push. We therefore write the probabilities $q(L_1|N_P)$ and $q(L_2|N_P)$ as being conditioned on N_P .

With these probabilities in hand, we now compute the disorder-averaged trap size and trapping time. Averaging Eq. (20) with Eqs. (24-25), we obtain

$$\langle A_T|N_P \rangle = 1 + \frac{2(N_P + 1)(1 - \rho)}{\rho}. \quad (26)$$

As expected, the average trap size increases with N_P , since a larger pushing capacity allows the walker to create larger gaps before becoming caged. Also, when $\rho = 1$, all lattice sites are occupied by obstacles except the origin, which is occupied by the walker. Hence, $\langle A_T|N_P \rangle = 1$ for $\rho = 1$, independent of N_P . As ρ is decreased, the typical gaps between obstacles become larger, allowing the walker to explore a larger region before caging; accordingly, Eq. (26) implies that $\langle A_T|N_P \rangle$ grows as obstacle density decreases and the mean diverges as $\rho \rightarrow 0$.

To find the disorder-averaged trapping time, we first notice that $\langle L_1 \rangle \sim \langle L_2 \rangle \sim (1 - \rho)/\rho$ following Eqs. (24-25). In the small-density limit, $\rho \rightarrow 0$, both L_1 and L_2 are typically large enabling us to use the large- $L_{1,2}$ asymptotics in Eq. (21). By contrast, in the high-density limit $\rho \rightarrow 1$, both L_1 and L_2 are typically zero. Such a configuration, as explained in Eq. (8), gives $n_T(L_1 = 0, L_2 = 0) = 0$. The leading order behavior will then be determined by $L_1 = 1, L_2 = 0$ or $L_1 = 0, L_2 = 1$. This reasoning allows us to use the expression of the average trapping time in Eq. (22). Employing Eqs. (24-25) to perform the disorder averaging of Eqs. (21-22), we obtain

$$\langle n_T|N_P \rangle \simeq \begin{cases} 4(N_P + 1)(1 - \rho), & \text{for } \rho \rightarrow 1, \\ (7 + 5N_P)(N_P + 1)/\rho^2, & \text{for } \rho \rightarrow 0. \end{cases} \quad (27)$$

The average trapping time vanishes as $\rho \rightarrow 1$ while it diverges as $\rho \rightarrow 0$. For $\rho = 1$, as explained above, the walker is trapped immediately at the origin, whereas for $\rho \rightarrow 0$ the increasingly large gaps delay caging and lead to a divergence in the trapping time.

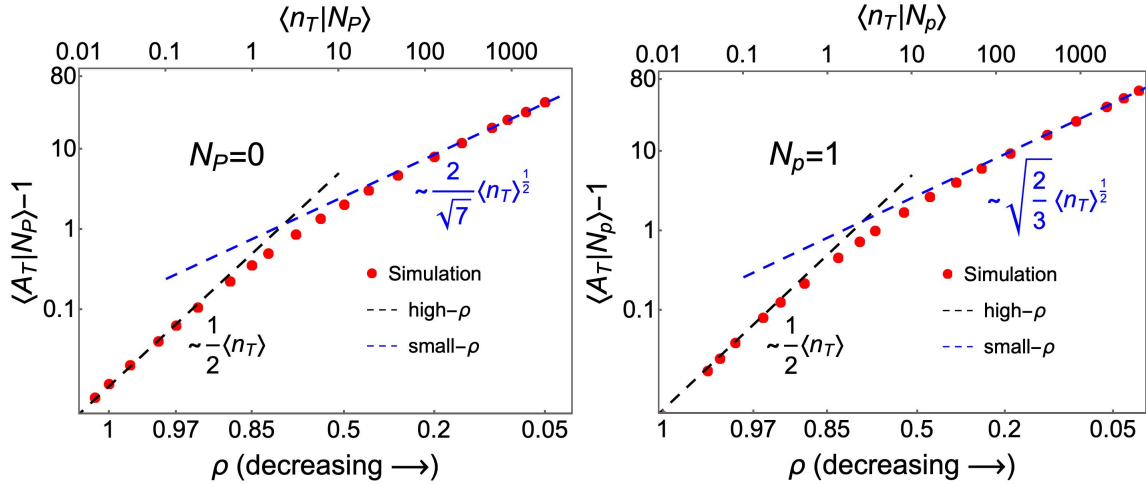


FIG. 5. Parametric-plot of $\langle A_T | N_P \rangle$ and $\langle n_T | N_P \rangle$ parametrised by ρ , illustrating their scaling-change behavior for the N_P -Sokoban walker with $N_P = 0$ (left) and $N_P = 1$ (right). In both panels, we plot density in the bottom axis while the averages $\langle A_T | N_P \rangle$ and $\langle n_T | N_P \rangle$ are plotted in the left and top axes respectively. The dashed lines are our theoretical results for small and high values of ρ given in Eq. (28).

Combining Eqs. (26-27), we yield the parametric relation

$$\langle A_T | N_P \rangle \simeq \begin{cases} 1 + \langle n_T | N_P \rangle / 2, & \text{for } \rho \rightarrow 1, \\ 2 \sqrt{\frac{(N_P+1)}{(7+5N_P)}} \langle n_T | N_P \rangle^{1/2}, & \text{for } \rho \rightarrow 0. \end{cases} \quad (28)$$

This equation reveals that, for Sokoban of any pushing capacity, the disorder-averaged trap size and trapping time exhibit a crossover in scaling – from a linear relation for ρ close to unity to a square-root dependence at small ρ . We later show that the linear high-density linearity persists in two dimensions, whereas the low-density regime changes drastically.

To validate our calculation, we perform numerical simulations following the method outlined in Appendix A. For different values of ρ , we obtain $\langle A_T | N_P \rangle$ and $\langle n_T | N_P \rangle$ from the simulations. These quantities are then presented in a parametric plot in Fig. 5 for $N_P = 0$ (left panel) and $N_P = 1$ (right panel). In each panel, $(\langle A_T | N_P \rangle - 1)$ is shown on the left axis, $\langle n_T | N_P \rangle$ on the top axis, and the corresponding density ρ along the bottom axis. We see that the change from the high-density linear behavior to the low-density power-law behavior is completely consistent with the numerical simulations for both values of N_P . Further notice that both $\langle A_T | N_P \rangle$ and $\langle n_T | N_P \rangle$ in Fig. 5 have a monotonic dependence on ρ . Upon decreasing density, both averages increase and diverge as $\rho \rightarrow 0$, which is an expected feature, as explained before. Changing the value of N_P does not qualitatively alter the monotonic behavior. This again is true only in 1d and one obtains a nonmonotonic behavior in the 2d setting due to the emergence of a self-trapping mechanism.

IV. DISORDER-AVERAGED SURVIVAL PROBABILITY

Having looked at the mean trapping time and trap size, let us examine the disorder-averaged survival probability

$$S(n | N_P) = \langle Q(n | L_1, L_2) \rangle_{L_1, L_2}, \quad (29)$$

with $Q(n | L_1, L_2)$ given in Eqs. (18-19). Since the statistics of L_1 and L_2 depend on N_P in Eq. (7), we again denote the survival probability $S(n | N_P)$ as being conditioned on N_P .

A. Survival probability for $N_P = 0$

We first look at the weak Sokoban limit, $N_P = 0$, where the walker does not push the obstacles. Therefore the values of L_1 and L_2 for a given initial obstacle configuration, as shown in Eq. (7), are determined by the positions of the first obstacles in the $+x$ and $-x$ directions. From the long-time expression in Eq. (18), it is clear that we require the joint probability $q(L, L_i | N_P = 0)$ of $L = (L_1 + L_2)$ and L_i for $i \in \{1, 2\}$. This joint probability can be calculated using Eqs. (24-25) for $N_P = 0$ as follows

$$\begin{aligned} q(L, L_i | N_P = 0) &= \sum_{L_{3-i}=0}^{\infty} q(L_i | N_P = 0) q(L_{3-i} | N_P = 0) \\ &\quad \times \delta_{L, L_i + L_{3-i}}, \\ &= \rho^2 (1 - \rho)^L \Theta(L - L_i). \end{aligned} \quad (30)$$

Using this expression to average Eq. (18), we get

$$S(n | N_P = 0) \simeq \frac{8\rho^2}{\pi} \sum_{L=1}^{\infty} (1 - \rho)^L \left(\frac{1}{2} + \frac{2L}{\pi} \right) e^{-\frac{\pi^2}{8L^2} n}. \quad (31)$$

Performing this summation analytically is challenging. However, for large n , we can introduce a quasi-continuous variable $u = 2\sqrt{2}L/\pi\sqrt{n}$ and transform the summation above into an integral

$$S(n|N_P = 0) \simeq \rho^2 \sqrt{8n} \int_0^\infty du \left(\frac{1}{2} + \frac{4\alpha u}{\pi\lambda} \right) e^{-\frac{1}{u^2} - 2\alpha u}, \quad (32)$$

$$\text{where } \alpha = \frac{\lambda\pi\sqrt{n}}{4\sqrt{2}}, \quad \lambda = |\ln(1 - \rho)|. \quad (33)$$

The integration over u can be carried out in terms of a Meijer-G function [29]

$$\int_0^\infty du u^m \exp\left(-\frac{1}{u^2} - 2\alpha u\right) = \frac{G_{0,3}^{3,0} \left(0, \frac{1+m}{2}, \frac{2+m}{2} \middle| \alpha^2 \right)}{2\sqrt{\pi}\alpha^{1+m}}. \quad (34)$$

Eq. (32) then becomes

$$S(n|N_P = 0) \simeq \sqrt{\frac{n\rho^4}{2\pi\alpha^2}} \left[G_{0,3}^{3,0} \left(0, \frac{1}{2}, 1 \middle| \alpha^2 \right) + \frac{8}{\pi\lambda} G_{0,3}^{3,0} \left(0, \frac{1}{2}, \frac{3}{2} \middle| \alpha^2 \right) \right]. \quad (35)$$

For $n\lambda^2 \gg 1$ (or equivalently $\alpha \gg 1$ from Eq. (33)), a further simplified expression for the survival probability can be obtained by using the asymptotic form of the Meijer-G function. This form is given in Eq. (D22) and using it we obtain

$$S(n|N_P = 0) \simeq \mathcal{K}_0(n) \exp\left(-\frac{3\pi^{2/3}}{2^{5/3}} (\lambda^2 n)^{\frac{1}{3}}\right), \quad (36)$$

$$\text{with } \mathcal{K}_0(n) = \frac{4\rho^2}{\sqrt{3\pi^3}\lambda^2} \left[16\alpha + \left(\frac{68}{9} + 2\pi\lambda \right) \alpha^{1/3} \right], \quad (37)$$

with α and λ given in Eq. (33). One can also get the same result by performing a saddle-point approximation directly in Eq. (32). This stretched-exponential result was announced before in Eq. (3).

Notice that the prefactor scales as $\mathcal{K}_0(n) \sim \sqrt{n}$ at large times. Comparing our result with the BVDV formula in Eq. (1), the two survival probabilities, $S(n|N_P = 0)$ and $\phi(n)$, are characterized by the same stretched exponent proportional to $\lambda^{2/3}n^{1/3}$, and share the same \sqrt{n} -scaling of the prefactor [24]. The difference, however, arises in the proportionality constant inside the exponential term. It takes the value $3\pi^{2/3}/2^{5/3}$ (≈ 2.0269) for $S(n|N_P = 0)$ and $3\pi^{2/3}/2$ (≈ 3.2175) for $\phi(n)$. A larger value for $\phi(n)$ means that it decays faster than $S(n|N_P = 0)$. The faster decay arises because $\phi(n)$ describes survival against a single obstacle, whereas $S(n|N_P = 0)$ corresponds to

survival against caging, a mechanism that necessarily involves more than one obstacle.

To compare Eq. (36) with numerical simulations, we plot

$$\chi(n|N_P = 0) \equiv \frac{-\log [S(n|N_P = 0)] + \log \mathcal{K}_0(n)}{\lambda^{2/3}n^{1/3}} \quad (38)$$

as a function of n in Fig. 6 (left panel). According to our theoretical result, $\chi(n|N_P = 0)$ should asymptotically converge to a constant value $\chi(n \rightarrow \infty|N_P = 0) = 3\pi^{2/3}/2^{5/3} \approx 2.0269$ independent of the density ρ . Indeed, in Fig. 6 (left panel), we have shown the simulation results of $\chi(n|N_P = 0)$ for different density values, and for all cases, the simulation data converge to the predicted constant value, 2.0269, indicated by the dashed black line. In this figure, we have also presented a comparison of our result with the BVDV formula in Eq. (1). According to this formula, $\lim_{n \rightarrow \infty} [-\ln \phi(n)/\lambda^{2/3}n^{1/3}] = 3\pi^{2/3}/2 \approx 3.2175$, which is shown by the dashed red line. Clearly, the red line is situated above the black line.

While the stretched-exponential decay is satisfied at long times, one can see deviations appearing at small and moderate values of n , see Fig. 6. To understand the behavior at moderate n , we will consider $Q(n|L_1, L_2)$ in Eq. (19), and take its expectation with respect to Eqs. (24-25). In Appendix D, we derive a simplified expression for the survival probability when $n\rho^2 \ll 1$

$$S(n|N_P = 0) \simeq 1 - n\rho^2, \quad \text{for } n\rho^2 \ll 1. \quad (39)$$

In Fig. 7 (left panel), we show the survival probability in both the intermediate-time and long-time regimes. We find that the stretched-exponential form shows a good agreement with the numerical simulations when $S(n|N_P = 0) \leq 0.1$. The agreement emerges even before entering into the regime of extremely rare events where $S(n|N_P = 0)$ is extremely small. This is largely due to the fact that the prefactor $\mathcal{K}_0(n)$ is known exactly, as given in Eq. (37), allowing for a good agreement even when n is not too large.

For $S(n|N_P = 0)$ close to unity, however, the stretched-exponential expression is not accurate and we observe deviations in Fig. 7. In this regime, the moderate-time expression in Eq. (39) governs the survival dynamics, especially at small densities. This is demonstrated in the inset of the figure where we have plotted $(1 - S(n|N_P = 0))$ vs $n\rho^2$ for two different densities. Our analytical result predicts a linear relationship that is independent of the density when $n\rho^2 \ll 1$. Indeed, the simulation data is consistent with this prediction.

Before closing this discussion, we compare our intermediate time result with Rosenstock's approximation for $\phi(n)$ in Eq. (2). While $(1 - \phi(n)) \sim \sqrt{n\rho^2}$, our result is clearly different. Thus, although, both $S(n|N_P = 0)$ and

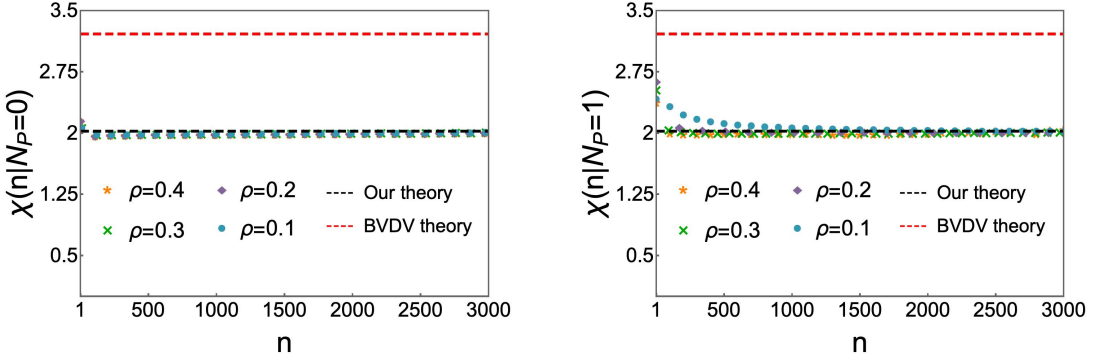


FIG. 6. Illustration of the long-time stretched-exponential decay of the survival probability $S(n|N_P)$ for the one-dimensional $N_P = 0$ (left panel) and $N_P = 1$ (right panel). The function $\chi(n|N_P)$, defined in Eqs. (38) and (43), is obtained from numerical simulation for different density values (represented by different symbols). For all values, the data, at large n , converge to a constant given by our theoretical calculation and shown by the black dashed line in both panels. For comparison, we have also presented in red dashed line the BVDV result in Eq. (1): $\lim_{n \rightarrow \infty} \left[-\ln \phi(n) / \lambda^{2/3} n^{1/3} \right] = 3\pi^{2/3}/2 \approx 3.2175$. We do not use any fitting parameter in this figure.

$\phi(n)$ show similar stretched-exponential decay at large n as far as the time dependence is concerned, their intermediate time behaviors are quite different.

B. Survival probability for $N_P = 1$

We next look at the Sokoban with pushing parameter $N_P = 1$, the one-dimensional version of the model introduced by Reuveni et al. [14, 15] (since $N_P = 0$ is not really a Sokoban). As explained in Eq. (7), the values of L_1 and L_2 are now determined by the positions of the second obstacles in the $+x$ and $-x$ directions. For this case also, the survival probability can be computed in the same manner. As shown in Appendix D 2, the moderate-time behavior of the disorder-averaged survival probability is

$$S(n|N_P = 1) \simeq 1 - \frac{n^2 \rho^4}{8}, \quad \text{for } n\rho^2 \ll 1, \quad (40)$$

It is important to emphasize that this expression is derived using $Q(n|L_1, L_2)$ in Eq. (19), which itself holds only at intermediate times. Consequently, Eq. (40) is expected to be valid only for moderate values of n but with small ρ so that $n\rho^2 \ll 1$. Under these conditions, $S(n|N_P = 1)$ decreases quadratically which is very different from the linear decrease for the weak Sokoban limit ($N_P = 0$) in Eq. (39). This implies that the survival probability remains closer to unity for the $N_P = 1$ case than for the $N_P = 0$ case. The enhanced survival in the former arises from the enhanced pushing capability, which allows the walker to avoid getting caged in a situation that would otherwise cage a weak Sokoban walker.

The late-time survival probability for $N_P = 1$ can also be obtained by following the same steps as for $N_P = 0$

in Eq. (36). We therefore relegate the details to Appendix D 1, focusing on the regime $n\lambda^2 \gg 1$, where we find

$$S(n|N_P = 1) \simeq \mathcal{K}_1(n) \exp \left(-\frac{3\pi^{2/3}}{2^{5/3}} (\lambda^2 n)^{1/3} \right). \quad (41)$$

The prefactor $\mathcal{K}_1(n)$ also depends on n and has a rather lengthy expression which is given in Eq. (D28). Its leading order expression in n is

$$\mathcal{K}_1(n) \simeq \frac{2^{19/6} (4 - \pi) \rho^4}{\sqrt{3\pi^{7/6}} \lambda^{5/3}} n^{7/6}, \quad (42)$$

with $\lambda = |\ln(1 - \rho)|$. We again see the survival probability $S(n|N_P = 1)$ decays in a stretched-exponential manner at late times, with the exponent $1/3$, same as the BVDV formula for $\phi(n)$ in Eq. (1). Increasing the pushing strength from $N_P = 0$ to $N_P = 1$ does not change the long-time stretched-exponential relaxation. The effect of N_P , however, can be found in the prefactor outside of this stretched-exponential decay. While it scales as $\mathcal{K}_0(n) \sim n^{1/2}$ for $N_P = 0$, the prefactor has a different scaling of the form $\mathcal{K}_1(n) \sim n^{7/6}$ for the Sokoban model with $N_P = 1$.

We next present the comparison of Eq. (41) for $S(n|N_P = 1)$ with numerical simulations. For this, we again define the quantity

$$\chi(n|N_P = 1) \equiv \frac{-\log [S(n|N_P = 1)] + \log \mathcal{K}_1(n)}{\lambda^{2/3} n^{1/3}}. \quad (43)$$

and plot it as a function of n . According to our calculation, this quantity should converge to $\chi(n \rightarrow \infty|N_P = 1) = 3\pi^{2/3}/2^{5/3} \approx 2.0269$ independent of the density. Fig. 6 (right panel) presents the simulation results for $\chi(n|N_P = 1)$ for different values of density ρ . For all

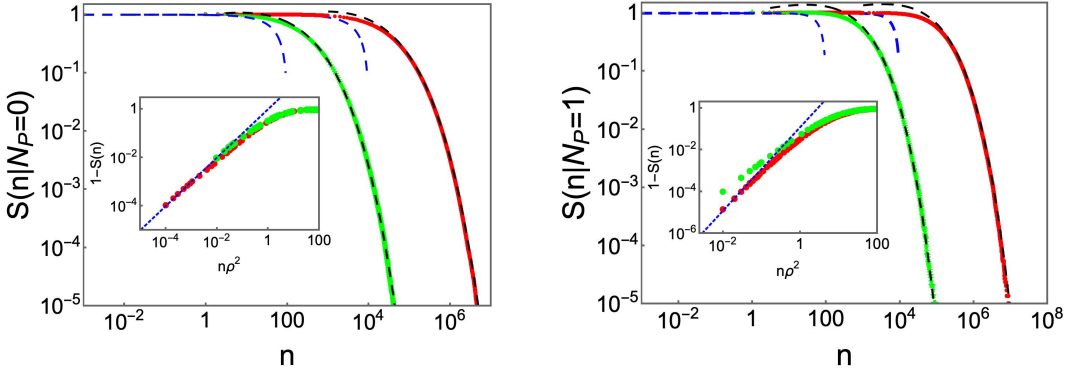


FIG. 7. Survival probability $S(n|N_P)$ for the one-dimensional N_P -Sokoban model with $N_P = 0$ (left panel) and $N_P = 1$ (right panel). Numerical simulations corresponding to $\rho = 0.01$ (red) and $\rho = 0.1$ (green) are compared with the theoretical results at moderate and long times. For $N_P = 0$, black dashed line corresponds to the long-time asymptotic expression in Eq. (36) while the blue line represents the intermediate-time expression in Eq. (39). Similarly, for $N_P = 1$, these are given in Eqs. (40) and (41) respectively. Insets in both panels present a magnified view of the intermediate-time comparison. Here, we have plotted $(1 - S(n|N_P))$ vs $n\rho^2$ for the same two densities. According to our theoretical analysis, $(1 - S(n|N_P))$ grows linearly and quadratically with $n\rho^2$ (with $n\rho^2 \ll 1$) for $N_P = 0$ and $N_P = 1$, respectively. Indeed, for both cases, the simulation data (shown by symbols) agree well with the theoretical predictions. Deviation in the right inset for $\rho = 0.1$ arises because our derivation assumes the limit of small $n\rho^2$ while keeping n moderately large. While this condition is easily satisfied at very low densities, it becomes increasingly difficult to achieve as ρ increases.

densities considered, the simulation data converge to the same constant value in the large- n limit. This observation is in excellent agreement with the theoretical result. Also, a comparison with the BVDV result in Eq. (1) is shown in this figure by the red dashed line. This line is significantly above $\chi(n \rightarrow \infty|N_P = 1)$, indicating that $\phi(n)$ has a faster decay than $S(n|N_P = 1)$.

We have also compared the moderate-time and long-time behaviors with numerical simulations in Fig. 7 (right panel). This comparison, similar to that performed for the $N_P = 0$ case, shows that the long-time expression in Eq. (41) works quite well for the survival dynamics except when $S(n|N_P = 1)$ is close to unity. There, our intermediate-time result in Eq. (40) gives a better approximation specially for small densities, see the inset in the figure. Notice that in the inset, the simulation data for $\rho = 0.1$ do not match with Eq. (40) while for $\rho = 0.01$, they match. This occurs because our derivation assumes the limit of $n\rho^2 \ll 1$ while keeping n moderately large. While this condition is easily satisfied at very low densities, it becomes increasingly difficult to achieve as ρ increases.

C. General survival probability: a large-deviation analysis

For both chosen values of N_P , we saw that the long-time exponent characterizing the survival probability is same as the BVDV formula. This naturally raises the question of what happens for general N_P . As mentioned before in Eq. (5), the survival probability for $N_P \gg 1$ admits a large-deviation form. We now derive this result.

For general N_P , the probability of L_i with $i \in \{1, 2\}$ is given in Eqs. (24-25). Substituting $L_i = N_P y_i$ and then

performing the Stirling approximation

$$\ln N_P! = N_P \ln N_P - N_P, \quad \text{for } N_P \gg 1, \quad (44)$$

we can write a large-deviation form [30-32]

$$q(L_i = N_P y_i | N_P \gg 1) \sim \exp [-N_P \Lambda(y_i)], \quad (45)$$

with function $\Lambda(y)$ defined as

$$\Lambda(y) = y \ln y - (1 + y) \ln(1 + y) - y \ln(1 - \rho) - \ln \rho. \quad (46)$$

Next, we average the conditional survival probability $Q(n|L_1, L_2)$ in Eq. (18) over L_1 and L_2

$$S(n|N_P) = \sum_{L_1=0}^{\infty} \sum_{L_2=0}^{\infty} Q(n|L_1, L_2) q(L_1|N_P) q(L_2|N_P). \quad (47)$$

This expression, with $Q(n|L_1, L_2)$ from Eq. (18), is valid for large n but any arbitrary value of N_P . For $N_P \gg 1$, it can be expressed as

$$S(n|N_P \gg 1) \sim \int_0^{\infty} dy_1 \int_0^{\infty} dy_2 \sin \left(\frac{\pi y_1}{2(y_1 + y_2)} \right) \times \exp \left[-N_P \Psi \left(\frac{n}{N_P^3}, y_1, y_2 \right) \right], \quad (48)$$

where

$$\Psi(\omega, y_1, y_2) = \frac{\pi^2 \omega}{8(y_1 + y_2)^2} + \Lambda(y_1) + \Lambda(y_2). \quad (49)$$

From Eq. (48), it now follows that the survival probability admits a large-deviation form in the joint limit $N_P \gg 1, n \gg 1$ keeping the ratio $n/(N_P)^3$ fixed

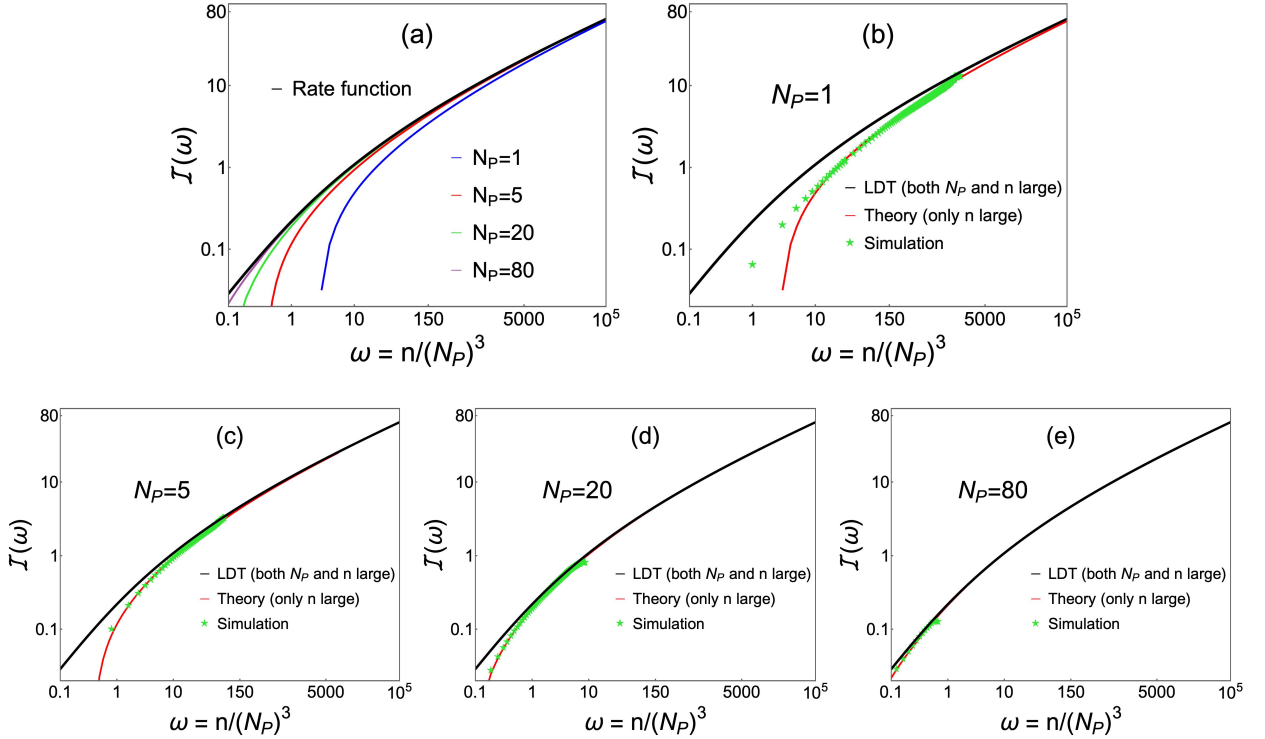


FIG. 8. Rate function $\mathcal{I}(\omega)$ is plotted as a function of $\omega = n / (N_P)^3$ for $\rho = 0.5$. In panel (a), the solid black line represents the rate function in Eq. (53) based on the large-deviation theory (LDT), which is valid for $n \gg 1$, $N_P \gg 1$ with ω fixed. It is compared with $[-\ln S(n|N_P) / N_P]$ for different N_P (shown by coloured lines) and $S(n|N_P)$ determined in Eq. (47). Recall that this expression is valid for large n but arbitrary N_P . Therefore, we see a departure between them at small and moderate N_P . However, as N_P is increased, the two expressions show a better agreement. In panels (b)-(e), the two theoretical results in Eqs. (47) and (53) are compared with the numerical simulations (shown by green symbols).

$$\lim_{\substack{N_P \gg 1, n \gg 1 \\ \omega = n / (N_P)^3 \text{ fixed}}} \frac{-\ln S(n|N_P)}{N_P} = \mathcal{I}(\omega), \quad (50)$$

which was also announced before in Eq. (5). The rate function $\mathcal{I}(\omega)$ is given by the minimization of $\Psi(\omega, y_1, y_2)$ with respect to both y_1 and y_2

$$\mathcal{I}(\omega) = \min_{y_1, y_2} \Psi(\omega, y_1, y_2). \quad (51)$$

By taking the derivative of Eq. (49) and setting it to zero, it turns out that the values of y_1 and y_2 (say \tilde{y}_1 and \tilde{y}_2) corresponding to the minimization are exactly the same ($\tilde{y}_1 = \tilde{y}_2 = \tilde{y}$) and it is governed by the equation

$$-\frac{\pi^2 \omega}{32 \tilde{y}^3} + \ln \tilde{y} - \ln(1 + \tilde{y}) - \ln(1 - \rho) = 0. \quad (52)$$

This equation can be numerically solved to generate $\tilde{y}(\omega)$ as a function of ω and inserting this solution in Eq. (51) gives the rate function

$$\mathcal{I}(\omega) = \frac{\pi^2 \omega}{32 \tilde{y}(\omega)^2} + 2\Lambda(\tilde{y}(\omega)), \quad (53)$$

where $\Lambda(\tilde{y}(\omega))$ is given in Eq. (46). Eqs. (52) and (53) completely characterize the exact large-deviation rate function describing the survival probability $S(n|N_P)$. It also turns out to be possible to find the asymptotic expressions of the rate function analytically. For this, we solve Eq. (52) in the limits of large and small ω to get

$$\begin{aligned} \tilde{y}(\omega) &\simeq \frac{(1 - \rho)}{\rho}, & \text{for } \omega \rightarrow 0, \\ &\simeq \frac{\pi^{2/3} \omega^{1/3}}{2^{5/3}}, & \text{for } \omega \rightarrow \infty. \end{aligned} \quad (54)$$

Substituting them in Eq. (53), we obtain the asymptotic expressions of $\mathcal{I}(\omega)$ as quoted before in Eq. (6). In terms of n , this translates to

$$S(n|N_P \gg 1) \sim \begin{cases} \exp\left(-\frac{\pi^2 \rho^2 n}{32(1-\rho)^2 (N_P)^2}\right), & \text{for } n \ll (N_P)^3 \\ \exp\left(-\frac{3\pi^{2/3} \lambda^{2/3}}{2^{5/3}} n^{1/3}\right), & \text{for } n \gg (N_P)^3 \end{cases} \quad (55)$$

indicating a change from an exponential decay of the survival probability to the stretched-exponential decay at very large times. Interestingly, the long-time stretched-

exponential form is independent of N_P and is exactly the same as for the Sokoban models with $N_P = 0$ and $N_P = 1$; see Eqs. (36) and (41) respectively. Therefore, in 1d, the long-time stretched-exponential decay of the survival probability is completely universal for any N_P and belongs to the BVDV universality class of the classical trapping problem in Eq. (1).

Let us heuristically try to understand this universality. Recall that for any value of N_P much smaller than the overall system size (due to the finite pushing ability), the motion is confined to a finite interval of length L for a given initial obstacle configuration. The statistics of L , in turn, depends on how many obstacles the walker is allowed to push. For a given N_P , the probability of L can be written as $h(\rho, L, N_P) e^{-\lambda L}$ where $\lambda = |\ln(1 - \rho)|$ and $h(\rho, L, N_P)$ is a polynomial function in L that depends on the value of N_P . One can verify this form using the exact probability in Eq. (24) also. The factor $e^{-\lambda L}$, on the other hand, does not depend on N_P . For small gaps, $L \ll 1/\lambda$, this factor is almost unity and only $h(\rho, L, N_P)$ controls the behavior of the survival probability. However, for large L , which dictates the long-time behavior, the exponential factor is dominant and the function $h(\rho, L, N_P)$ gives only the sub-leading effect. For a given value of L , we saw in Eq. (18) that the survival probability at long time decays as $\sim \exp(-\pi^2 n/8L^2)$. When we average this exponential decay over $e^{-\lambda L}$, the disorder-averaged survival probability has the same stretched-exponential relaxation as quoted in the second line of Eq. (55).

Fig. 8(a) represents a comparison of our rate function $\mathcal{I}(\omega)$ in Eq. (53) with $[-\ln S(n|N_P)/N_P]$ where $S(n|N_P)$ is determined using Eq. (47). Recall that the latter expression is valid for large n but arbitrary N_P . On the other hand, Eq. (53) is based on the large-deviation calculation which is valid under the joint limit $n \gg 1$, $N_P \gg 1$ with the ratio $\omega = n/(N_P)^3$ held fixed. Therefore, the two expressions, as expected, show deviations at small values of N_P . However, as N_P is increased, they show better agreement, establishing the validity of Eq. (53). Next in panels (b)-(e) of the same figure, we have also compared them with the numerical simulations. The simulation data, shown in green, is completely consistent with Eq. (47), which is shown in red. Deviations appear only for small n , since our theoretical expression is not valid there. From these figures, it is also clear that sampling larger ω values for large N_P in simulation is computationally challenging [see panel (e)]. This requires performing Monte Carlo simulations at time scales much greater than $(N_P)^3$, where the survival probability is extremely small. As a result, a very large sample size is needed to accurately capture these rare events. The range of ω over which we can compare the simulation with our theoretical expressions quickly decreases as we increase N_P . However, within this range, we see a good agreement between simulation and Eq. (47) and both of them converge to the rate function $\mathcal{I}(\omega)$ in Eq. (53) on increasing N_P (shown in black).

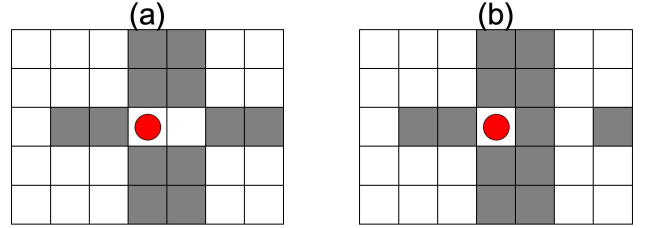


FIG. 9. Panels (a) and (b) schematically show the initial configurations of obstacles as gray blocks and walker in red. A single vacancy located either adjacent to the walker or at a next-nearest-neighbor site determine the trapping time of the Sokoban model in Eq. (58) for $\rho \rightarrow 1$.

V. SOKOBAN MODEL IN TWO DIMENSION

In one dimension, we have a universal long-time stretched-exponential relaxation of the survival probability for any N_P . The stretch exponent 1/3 matches with the BVDV theory in Eq. (1). In this section, we analyze the trapping aspects of the two-dimensional Sokoban model and its variant, the G-Sokoban model, introduced in Sec. II.

A. Mean trapping time

Let us first look at the average of n_T . Recall that, by our definition, the walker, for a given realization of the initial obstacle configuration, is considered trapped when the number of distinct visited lattice sites saturates to a finite value. The observable n_T denotes the time at which this saturation is first reached. Analytical calculations in two dimensions turn out to be considerably more challenging than in the one-dimensional case. However, for densities close to unity ($\rho \rightarrow 1$), we can calculate the leading order behavior of $\langle n_T \rangle$ in $(1 - \rho)$.

To see this, let us consider $\rho = 1$ so that all lattice sites – except the origin where the walker is initially placed – are occupied with obstacles. So the Sokoban is trapped right at the beginning, *i.e.* $\langle n_T \rangle = 0$. On the other hand, when ρ is close to, but not exactly equal to unity, the leading-order behavior is determined by the presence of a single vacancy. Two type of configurations can arise, as shown schematically in Fig. 9(a) and (b). In both cases, one needs at least twelve lattice sites with obstacles and one site that is vacant. The vacant site may be adjacent to the walker [panel (a)] or located at a next-nearest-neighbor position [panel (b)], such that the walker can jump by pushing the obstacle into this vacant site. Moreover, this vacant site can be located in any of the four nearest neighbors of the walker, which gives a degeneracy of 4. Combining everything together, the probability of observing such initial configurations of obstacles is

$$\mathbb{P} = 8\rho^{12}(1 - \rho). \quad (56)$$

Given this configuration, the trapping time can, in principle, take all possible positive integer values. For exam-

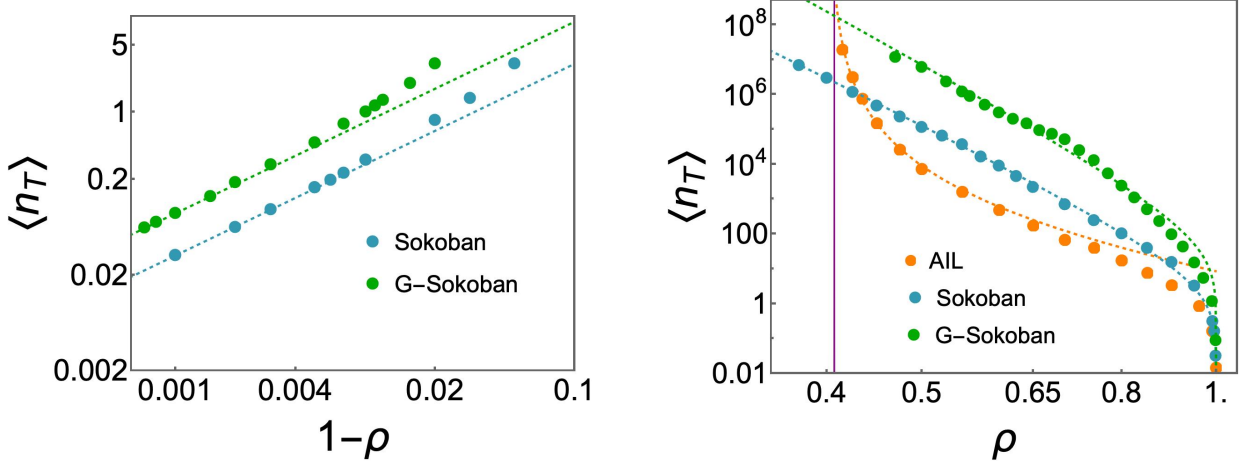


FIG. 10. *Left panel:* Mean trapping time $\langle n_T \rangle$ as a function of $(1 - \rho)$ for the two-dimensional Sokoban and G-Sokoban models when ρ close to unity. The dots are obtained from the simulations while dashed lines are the high-density expressions in Eq. (58) for Sokoban and in Eq. (59) for G-Sokoban. *Right panel:* Here, we show $\langle n_T \rangle$ across all the accessible density range. Once again, the dots are from the numerical simulation. The blue and the green lines are fits to the simulation data, as explained in Eqs. (60) and (61) respectively. For comparison, we have also shown in orange the simulation results for the AIL model, which diverges around the percolation threshold, $\rho \rightarrow \rho_c$. We show in Appendix E that the divergence around ρ_c is described by $\langle n_T \rangle \sim (\rho - \rho_c)^{-3.8373}$ (also shown by the orange line in the right panel).

ple, $n_T = 1$, when the Sokoban successfully jumps on the very first attempt. The probability of such a successful jump is $1/4$. Similarly $n_T = 2$ when the first jump attempt is unsuccessful but the second attempt succeeds. The probability of this is $3/4 \times 1/4$. Proceeding in this way, we can write the mean of n_T as

$$\langle n_T \rangle_{\text{sok}} \simeq \mathbb{P} \left[\frac{1}{4} \times 1 + \frac{3}{4} \times \frac{1}{4} \times 2 + \dots + \dots + \left(\frac{3}{4} \right)^{m-1} \times \frac{1}{4} \times m + \dots \right], \quad (57)$$

where we have used the subscript ‘sok’ to indicate the model (this notation will be adopted throughout the remainder of the paper). It is possible to perform the above summation analytically and obtain

$$\langle n_T \rangle_{\text{sok}} \simeq 32(1 - \rho), \quad \text{as } \rho \rightarrow 1. \quad (58)$$

The same treatment for the G-Sokoban model yields

$$\langle n_T \rangle_{\text{Gsok}} \simeq 88(1 - \rho), \quad \text{as } \rho \rightarrow 1. \quad (59)$$

Our analysis thus reveals that the mean trapping time for both models vanishes linearly in $(1 - \rho)$, albeit with different prefactors. For a given value of ρ close to unity, we find that the G-Sokoban model has the highest trapping time, followed by the Sokoban walker. Due to the highest mobility of the obstacles in the G-Sokoban model, the traps can be relatively large, and the walker thus requires a longer time to get trapped in these larger traps. In the left panel of Fig. 10, we present a comparison between our theoretical result and the numerical simulations, and find an excellent agreement between them for both models.

1. Finite $\langle n_T \rangle$

Beyond $\rho \rightarrow 1$, we have performed numerical simulations to study the average trapping time for other values of ρ . We refer to Appendix A for details on the numerical simulations. The right panel of Fig. 10 shows a plot of $\langle n_T \rangle$ as a function of ρ for both models. For comparison, we have also shown the simulation results for the AIL model. One can clearly observe that $\langle n_T \rangle$ diverges for the AIL model (shown in orange) as the density approaches the percolation threshold, $\rho \rightarrow \rho_c^+ (\approx 0.407)$. For $\rho \leq \rho_c$, a spanning cluster of vacant sites of infinite size emerges, and it takes an infinite time for the AIL walker to sample all sites within this cluster [3]. This leads to the divergence of $\langle n_T \rangle$ for $\rho \leq \rho_c$ (see Appendix E for more details).

On the other hand, we do not observe any divergence for the Sokoban and G-Sokoban models, at least within the range of density values for which we can perform our simulations. The minimum density for which we could reliably run our simulation is $\rho = 0.375$ for the Sokoban model and $\rho = 0.47$ for the G-Sokoban model. At these densities, the average trapping time is on the order of $\sim 10^7$, and to accurately probe such an average time, we need a total simulation time of the order of $\tau_{\text{sim}} \sim 10^8$. Decreasing ρ further increases τ_{sim} , and to avoid the finite system size effects at such large time values, we also need to increase the total lattice size (see Appendix A). Both of these factors contribute to making the simulations significantly more expensive.

A fitting analysis of the simulation data within the accessible density regime reveals that the mean trapping

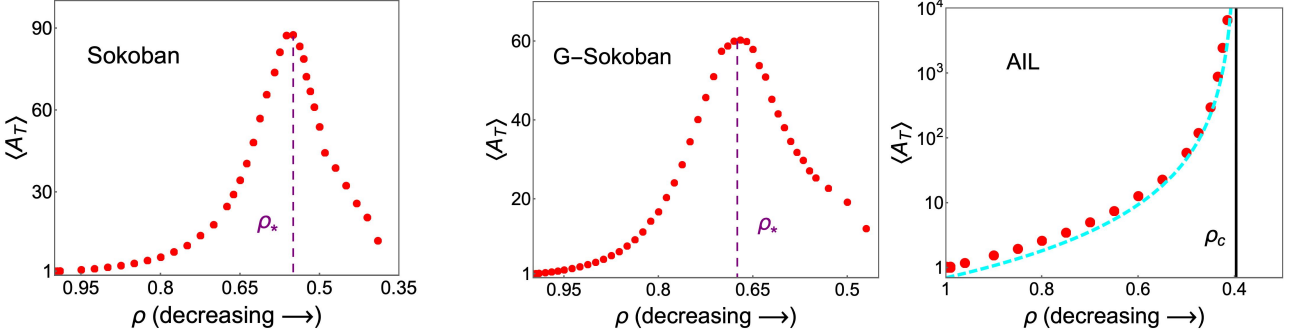


FIG. 11. Average trap size $\langle A_T \rangle$ is plotted as a function of ρ for the two-dimensional Sokoban (left), G-Sokoban (middle) and AIL (right) models. Across all panels, the red dots are the simulation data. For the Sokoban and G-Sokoban models, the plot is nonmonotonic with the maximum value occurring at ρ_* (shown by purple dashed line). Based on simulations, we estimate $\rho_* \approx 0.55$ for the Sokoban model and $\rho_* \approx 0.675$ for the G-Sokoban model, where the corresponding maximal mean trap sizes are approximately 87 and 60, respectively. In contrast, the plot for the AIL model is monotonic with $\langle A_T \rangle$ diverging at $\rho_c \approx 0.407$. As shown in Appendix E, the divergence around $\rho \gtrsim \rho_c$ is described by $\langle A_T \rangle \sim (\rho - \rho_c)^{-43/18}$ and shown by the cyan line in the right panel.

time for the Sokoban model satisfies a scaling

$$\langle n_T \rangle_{\text{sok}} \sim \frac{(1 - \rho)}{\rho^{\gamma_{\text{sok}}}}, \quad (60)$$

with the exponent estimated to be $\gamma_{\text{sok}} \approx 13.17 \pm 0.1$. The error is estimated through least squares fitting of the simulated data. This fitting result is shown by the blue dashed line in the right panel of Fig. 10. In this figure, we clearly see that $\langle n_T \rangle_{\text{sok}}$ remains finite even past the percolation threshold. This supports the hypothesis that the percolation transition is lost for the two-dimensional Sokoban random walk.

The finiteness of the mean trapping time $\langle n_T \rangle_{\text{sok}}$ suggests that trapping in the Sokoban model does not occur merely through the exploration of a cluster of vacant sites. Later, we will show that, at low densities, a self-trapping mechanism emerges for the Sokoban walker, in which it gets dynamically localized by a creating a cage for itself.

Similarly, we have repeated the fitting treatment for the G-Sokoban model and found

$$\langle n_T \rangle_{\text{Gsok}} \sim \frac{(1 - \rho)}{\rho^{\gamma_{\text{Gsok}}}}, \quad (61)$$

with a different exponent $\gamma_{\text{Gsok}} \approx 14.93 \pm 0.4$. This is again shown in Fig. 10 (right panel). Once again, we do not find any divergence of the average trapping time within the considered density regime.

B. Trap size

We now turn our focus to the size of the trap. Remember that the trap size is defined as the number of vacant sites enclosed by the trap. As before, the case of $\rho \rightarrow 1$ turns out to be perturbatively solvable for $\langle A_T \rangle$. When $\rho = 1$, all lattice sites except the origin are occupied by obstacles, resulting in a trap size of $\langle A_T \rangle = 1$.

When $\rho \rightarrow 1$, the leading order correction to this is determined by one single vacancy, as indicated in Fig. 9. These configurations are characterized by $A_T = 2$ and their probability is given in Eq. (56). Following this expression, we obtain the mean trap size

$$\langle A_T \rangle_{\text{sok}} \simeq 1 + 8(\rho - 1), \quad \text{as } \rho \rightarrow 1. \quad (62)$$

Similarly, for the G-Sokoban model, we find

$$\langle A_T \rangle_{\text{Gsok}} \simeq 1 + 12(\rho - 1), \quad \text{as } \rho \rightarrow 1 \quad (63)$$

Combining these results with our previous analysis of $\langle n_T \rangle$, we find a linear relation for both models

$$\langle A_T \rangle_{\text{sok}} \simeq 1 + \frac{1}{4} \langle n_T \rangle_{\text{sok}}, \quad (64)$$

$$\langle A_T \rangle_{\text{Gsok}} \simeq 1 + \frac{3}{22} \langle n_T \rangle_{\text{Gsok}} \quad (65)$$

These relations are valid only for ρ close to unity, where both averages are small. It is also reminiscent of what was rigorously proven in one dimension (see Eq. (28) and Fig. 5). The universality of the high-density linearity across different models and dimensions suggests that the underlying trapping mechanism in the high density regime is the same for all of them. In particular, the Sokoban walker explores the small void surrounding its initial position. It can slightly enlarge this void by displacing nearby obstacles, but the extent of this expansion is limited due to the high obstacle density. Ultimately, the walker becomes trapped once all vacant sites within this locally reshaped region have been visited. In contrast, a qualitatively different self-trapping mechanism emerges for both models at low densities, as we now illustrate.

1. Self-trapping and nonmonotonic $\langle A_T \rangle$

We plot $\langle A_T \rangle$ as a function of ρ in Fig. 11 using numerical simulations. For both models, we see in the left

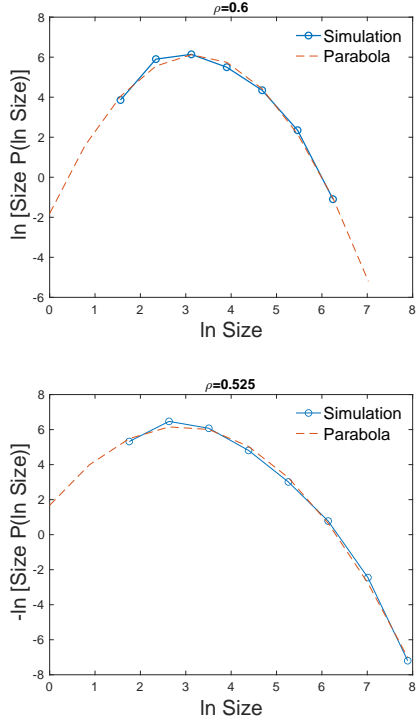


FIG. 12. The trap size distribution: Shown is the measured $\ln[A_T P(\ln A_T)]$ vs. $\ln A_T$ for $\rho = 0.6$ (top panel) and $\rho = 0.525$ (bottom panel) for two-dimensional Sokoban model. Also shown is the best-fit parabola in the two cases, showing excellent agreement.

and the middle panels that the $\langle A_T \rangle$ vs ρ plot is non-monotonic. Starting from densities close to unity, the mean trap size starts to increase on decreasing the density. The growth of the mean trap size continues only till a characteristic density ρ_* , at which point $\langle A_T \rangle$ achieves its (finite) maximum value. Below this threshold, $\rho < \rho_*$, we find a turnover behavior in which the mean trap size decreases with decreasing ρ . Based on numerical simulations, we find the turnover density to be $\rho_* \approx 0.55$ for the Sokoban model and $\rho_* \approx 0.675$ for the G-Sokoban model. The corresponding maximum values of the average trap size are approximately 87 and 60, respectively.

By contrast, for the AIL model, the dependence of $\langle A_T \rangle$ on ρ is monotonic with divergence at the percolation threshold ρ_c ; see the right panel in Fig. 11. As explained above, this divergence arises due to the emergence of an infinite cluster of vacant sites at ρ_c .

So what gives rise to nonmonotonicity for models with pushing ability? Consider again the high-density limit $\rho \rightarrow 1$. In this regime, all sites, except for the origin occupied by the walker, are filled with obstacles. Consequently, the average trap size $\langle A_T \rangle = 1$. On slightly decreasing the density, a void of vacancies is created around the walker which increases the mean trap size $\langle A_T \rangle$. As ρ decreases further, the surrounding void grows larger, resulting in a continued increase in $\langle A_T \rangle$. For the AIL model, this trend will continue all the way till $\rho \rightarrow \rho_c^+$ at

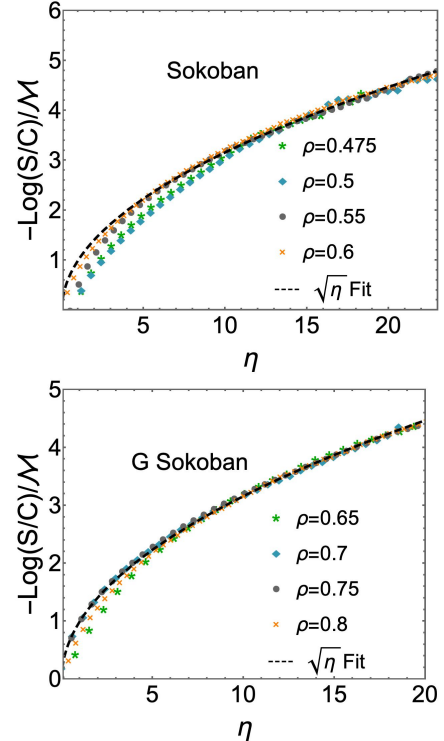


FIG. 13. Demonstration of the late-time stretched-exponential decay of the survival probability for two-dimensional Sokoban and G-Sokoban models. We have plotted $-\log [S(\eta)/C(\eta)]/\mathcal{M}(\rho)$ as a function of $\eta = n/\langle n_T \rangle$ using numerical simulations for different densities (shown by symbols). For both models at all densities, the numerical data converge to $\sqrt{\eta}$ form, as indicated by the dashed line when η is sufficiently large. To generate these plots, we have determined the average $\langle n_T \rangle$ from simulations, while the functions $C(\eta)$ and $\mathcal{M}(\rho)$ are estimated using a fitting procedure as explained in Appendix F.

which point $\langle A_T \rangle$ diverges.

However, the situation changes dramatically for the Sokoban and G-Sokoban models, where the walker can minimally push the obstacles. The growth trend continues only till the threshold ρ_* . Below this threshold, $\rho < \rho_*$, a qualitatively different trend emerges. Even when large voids are available for motion, the walker may encounter a rare region containing a manipulable arrangement of obstacles. This region, through successive pushing by the walker, can be gradually reorganized into a confining structure; see Fig. 2. This leads to the formation of a localized trap that was not pre-existing but dynamically constructed by the walker itself. As ρ continues to decrease, there are fewer manipulable obstacles, so that traps are harder to create, and smaller on average. This results in a turnover to decreasing trap size $\langle A_T \rangle$, making the overall relation nonmonotonic.

Note that at high densities, self-trapping is suppressed, as the Sokoban cannot substantially rearrange the obstacles due to the limited available space. However, at low densities, the available space allows the walker to move and push obstacles to create configurations that result

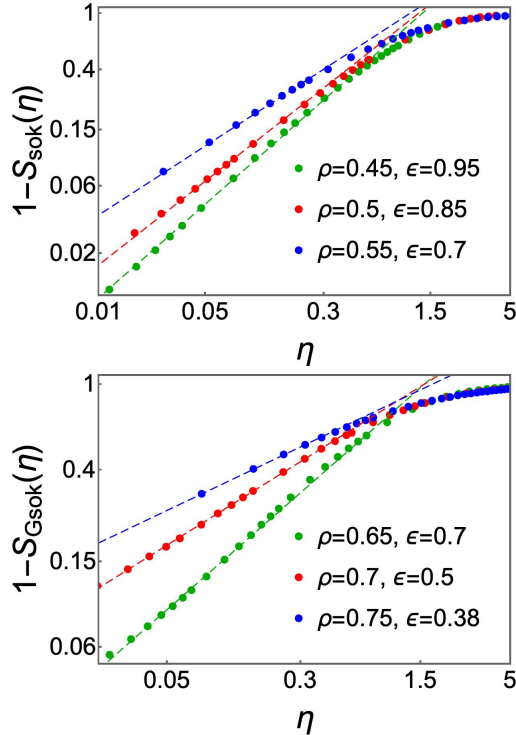


FIG. 14. Moderate-time behavior of the survival probability for two-dimensional Sokoban (top) and G-Sokoban (bottom) models. We have plotted $(1 - S(\eta))$ vs η using numerical simulations where $\eta = n/\langle n_T \rangle$. The dashed lines are the fits to the simulation data, and from these fits, we infer $(1 - S(\eta)) \sim \eta^{\epsilon(\rho)}$ when $\eta \ll 1$. The exponent ϵ , as quoted in the legends, depends on the density as well as on the models. Contrast this with $1d$ where the exponent is independent of the density for a given model.

in self-trapping. As a result, the Sokoban walker cannot percolate, as observed in [14], or equivalently, in the finiteness of $\langle A_T \rangle$ and $\langle n_T \rangle$ in our case. Nonetheless, it exhibits a trapping crossover, marked by a characteristic density ρ_* that separates two distinct regimes: a self-trapping regime at low density, where the walker becomes dynamically localized within a self-formed trap, and a pre-existing trapping regime at high density, where confinement arises from the initial arrangement of obstacles. This crossover is also observed in the G-Sokoban model highlighting its robustness and suggesting that self-trapping is a generic dynamical mechanism across a broad class of Sokoban-type walkers.

C. Trap Size Distribution

Above we considered the behavior of the mean trap size as a function of ρ . It is also interesting to consider the distribution of trap sizes. Running many realizations of the two-dimensional Sokoban model till trapping for a given ρ , we constructed the histogram of trap sizes and discovered that the distribution is well described by a

log-normal distribution

$$P(A_T) = \frac{1}{A_T \sigma \sqrt{2\pi}} \exp \left[-\frac{1}{2\sigma^2} \left(\ln \left(\frac{A_T}{\langle A_T \rangle} \right) + \frac{\sigma^2}{2} \right)^2 \right], \quad (66)$$

where σ is the variance of $\ln A_T$. To see the log-normal distribution, we plot $\ln[A_T P(\ln A_T)]$ against $\ln A_T$. For a log-normal distribution, this would yield a parabola. We show in Fig. 12 the results of implementing this for $\rho = 0.6$ and $\rho = 0.525$, together with the best fit parabola. We see that for both values of ρ the parabola gives an excellent fit. We have done this for densities in the range $0.475 < \rho < 0.6$ and found excellent fits to a log-normal distribution in all cases. It is an interesting challenge to understand the origin of this log-normal distribution.

D. Survival probability

We now turn our attention to the survival probability that the Sokoban random walker has not been trapped in dimension two. For the $1d$ case, we saw that the survival probability has the long-time stretched-exponential relaxation with exponent proportional to $\lambda^{2/3} n^{1/3}$ and belonged to the BVDV trapping universality class. For two-dimensional models, we first rescale time by the average trapping time and define

$$\eta = n/\langle n_T \rangle. \quad (67)$$

Based on extensive numerical simulations, we show in Fig. 13 that the late-time decay of the survival probability for both Sokoban and G-Sokoban models turns out to be

$$S_{\#}(\eta) \simeq C_{\#}(\eta) \exp \left(-\mathcal{M}_{\#}(\rho) \eta^{1/2} \right), \quad \text{for } \eta \gg 1. \quad (68)$$

Here, $\#$ stands for the sok or Gsok depending on the model. Comparing this form with the $\phi(n)$ in Eq. (1), we observe that the stretch exponent $1/2$ is same as the BVDV formula for both models. However unlike this formula, we do not have any analytical prediction of the functions $C_{\#}(\eta)$ and $\mathcal{M}_{\#}(\rho)$. Instead, both quantities are extracted numerically through a fitting procedure. For this, we plot $\log S(\eta)$ versus η for various densities and find that the resulting curves can be fitted with $\log S_{\#} = \log C_{\#} - \mathcal{M}_{\#}(\rho) \eta^{1/2}$. The coefficient $\mathcal{M}_{\#}(\rho)$ is then determined from the asymptotic slope in the large- η regime, while the prefactor $C_{\#}(\eta)$ is obtained by adjusting the vertical intercept to ensure a good fit across the appropriate range. More details of this fitting procedure are given in Appendix F. In particular, for $\mathcal{M}_{\#}(\rho)$, fol-

lowing this fitting procedure, we estimate

$$\mathcal{M}_\#(\rho) \approx \begin{cases} 0.0785 \langle n_T \rangle^{1/3}, & \text{for Sokoban,} \\ 0.55 \langle n_T \rangle^{1/10}, & \text{for G-Sokoban.} \end{cases} \quad (69)$$

With these estimates, we now proceed to plot $-\log [S(\eta)/C(\eta)]/\mathcal{M}(\rho)$ as a function of η in Fig. 13 using numerical simulations for different values of density. Regardless of the value, the rescaled curves for both models converge to the same asymptotic $\sqrt{\eta}$ form when η is large

Plugging the density dependence of the average trapping time via Eqs. (60) and (61) and converting from η back to the actual time n , we get

$$S(n) \sim \exp \left(-f_2(\rho) n^{1/2} \right), \quad \text{for } n \gg \langle n_T \rangle, \quad (70)$$

with

$$f_2(\rho) \sim \begin{cases} \rho^{\frac{\gamma_{\text{sok}}}{6}} / (1 - \rho)^{\frac{1}{6}}, & \text{for Sokoban,} \\ \rho^{\frac{2\gamma_{\text{Gsok}}}{5}} / (1 - \rho)^{\frac{2}{5}}, & \text{for G-Sokoban.} \end{cases} \quad (71)$$

Recall that $\gamma_{\text{sok}} \approx 13.17 \pm 0.1$ and $\gamma_{\text{Gsok}} \approx 14.93 \pm 0.4$. Therefore, we see that even in two dimensions, for both Sokoban and G-Sokoban models, $S(n)$ bears a resemblance to $\phi(n)$ in Eq. (1), as far as the exponent 1/2 is concerned. This suggests the BVDV trapping universality class even in two dimensions.

Finally, we have analyzed the intermediate time behavior of the survival probability and plotted $(1 - S(\eta))$ vs η in Fig. 14 for the two models. In 1d, we analytically proved that $(1 - S(\eta))$ scales as $\sim n\rho^2$ for $N_P = 0$ and as $\sim n^2\rho^4$ for $N_P = 1$. In 2d, in contrast, our simulation reveals

$$1 - S(\eta) \sim \eta^{\epsilon(\rho)} \quad (72)$$

where the exponent ϵ depends on ρ . For densities considered in Fig. 14, the value of the exponent is quoted in the legend. Moreover, for a given density, ϵ also depends on the model. Thus, the short-time behavior is sensitive to both density as well as the details of the underlying model.

VI. CONCLUSION AND OUTLOOK

In conclusion, we analyzed the trapping behavior of the Sokoban-type random walk in a disordered medium with obstacle density ρ , where the walker can locally modify its environment by pushing a few obstacles that block its path. Our goal was to understand how the limited pushing dynamics affects the nature of trapping in one and two dimensions. For this, we studied the following three quantities: (i) the disorder-averaged survival probability $S(n)$ that the walker has not yet been trapped until time n , (ii) the average trap size $\langle A_T \rangle$ and, (iii) the average trapping time $\langle n_T \rangle$.

We showed that the survival probability $S(n)$ for the Sokoban model has a stretched-exponential relaxation at late times, with stretch exponents 1/3 and 1/2 in one and two dimensions, respectively; see Figs. 7 and 13. The exponents are similar to the Balagurov-Vaks-Donsker-Varadhan (BVDV) formula for the reactive-trapping-based survival probability $\phi(n)$ described in Eq. (1). In one dimension, we proved that this result is valid for the general N_P -Sokoban model, in which the walker is capable of pushing up to an arbitrary N_P number of obstacles. For $N_P \gg 1$, the survival probability $S(n)$ is characterized by a large-deviation rate function and it exhibits an exponential decay for not too large n , before reverting to the same stretched-exponential decay at long times; see Eq. (55).

In two dimensions, we studied a variant of the Sokoban model, referred to as the G-Sokoban model, which features a modified pushing dynamics. Despite this modification, the survival probability $S(n)$ still exhibits a long-time stretched-exponential decay with a stretch exponent of 1/2.

While the long-time behavior of both survival probabilities, $S(n)$ and $\phi(n)$, display similarities, placing them in the same universality class, there are some differences also. In one dimension, both of them decay with an exponent proportional to $\lambda^{2/3}n^{1/3}$ at long times, but with markedly different proportionality constants: for $\phi(n)$ in Eq. (1), the constant is $3\pi^{2/3}/2 \approx 3.2175$, whereas for $S(n)$ in Eq. (55), it is $3\pi^{2/3}/2^{5/3} \approx 2.0269$ independent of N_P . Differences also appear in the algebraic prefactor multiplying the stretched-exponential term. For instance, in Eq. (42) for $S(n)$ with $N_P = 1$ this prefactor scales as $n^{7/6}$, while for $\phi(n)$ it scales as \sqrt{n} [24].

The moderate-time behaviors of $S(n)$ and $\phi(n)$ are also qualitatively different. For $\phi(n)$, the decay at moderate times is well described by the Rosenstock approximation: $(1 - \phi(n)) \sim \sqrt{n\rho^2}$ for $n\rho^2 \ll 1$ in one dimension (with moderate n), see Eq. (2). Contrarily, we find that $S(n)$ for the Sokoban model exhibits a much slower decrease in this regime, with $(1 - S(n)) \sim n\rho^2$ for $N_P = 0$ and $(1 - S(n)) \sim n^2\rho^4$ for $N_P = 1$. This highlights that despite similarities in the long-time exponents, the survival probabilities $S(n)$ for different values of N_P are very different.

We also reported a dynamical crossover in the underlying trapping mechanisms that replaces the classical percolation transition in the two-dimensional Sokoban and G-Sokoban models. Unlike in the AIL model, where trapping occurs due to geometric constraints imposed by the static disorder, the above crossover occurs due to the limited pushing ability of the walker. As a result, the average trap size exhibits a nonmonotonic dependence on the obstacle density ρ , as shown in Fig. 11. Starting from high density, it increases as ρ is decreased, achieving a maximum near a characteristic density ρ_* , and then decreases beyond this value. Based on numerical simulations, we estimated $\rho_* \approx 0.55$ for the Sokoban model and $\rho_* \approx 0.675$ for the G-Sokoban model. The crossover

density ρ_* separates two qualitatively distinct trapping mechanisms: at high densities, the walker is predominantly trapped by pre-existing obstacles in the environment, whereas at low densities, trapping arises primarily through a self-trapping mechanism, where the walker dynamically constructs its own confinement by reorganizing its local environment. This self-trapping mechanism prevents long-range transport in the Sokoban model.

Going forward, our work paves the way for several directions for future investigation. While analytical treatment is feasible in one dimension, extending such a treatment to two dimensions remains a significant open challenge. Many of our results in two dimensions are based on the fitting procedure and verifying these results through a more rigorous method is an important future challenge. On the computational side, although numerical simulation offers valuable insights in two dimensions, it becomes increasingly expensive at small densities and at long times. Standard numerical techniques based on simple sampling become inefficient in this regime due to the rarity of trapping events. Therefore, it remains an important open problem to develop efficient computational methodologies to probe the Sokoban model in the small-density regime. Another interesting future direction would be to replace the unbiased diffusive motion in the Sokoban model with sub-diffusive dynamics (e.g., via a continuous-time random walk framework) or directed diffusive motion or pushy random motion, and investigate how this affects the trapping behavior and the associated survival probability [33, 34].

ACKNOWLEDGMENT

The support of Israel Science Foundation's grant 2311/25 is gratefully acknowledged.

Appendix A: Details of the numerical simulations

Here we will present details of the numerical simulation followed to obtain various results in the paper. We take a square lattice of size \mathcal{N}^d , d being the dimension, and place a random walker at the center. The system size is typically chosen in the range $\mathcal{N} = 301\text{--}1001$ for $1d$ and $\mathcal{N} = 601\text{--}5001$ for $2d$ depending on the obstacle density ρ . Except at the center, which contains the walker, every other site (i, j) is characterized by an indicator function

$$\begin{aligned} \mathbb{I}(i, j) &= 1, \quad \text{with probability } \rho, \\ &= 0, \quad \text{with probability } (1 - \rho). \end{aligned}$$

to indicate the presence or absence of an obstacle at that particular site. For a given initial realization of the obstacles, we then evolve the system (walker + obstacles) according to the Sokoban dynamics, as discussed in Sec. II. To see whether the walker is trapped or not, we monitor the number of distinct sites $\Omega(n)$ that it has visited. For

a given realization, it is a monotonically increasing function of time and saturates only if the Sokoban is trapped. Otherwise, it continues to grow indefinitely. Therefore, by looking at $\Omega_{\text{sat}} = \Omega(n \rightarrow \infty)$, we can say whether the walker is trapped or not. When the walker is trapped, we define the trapping time, n_T , as the time at which $\Omega(n)$ saturates to its $\Omega(n \rightarrow \infty)$ value for the first time (see Fig. 2). In simulation, we cannot have an infinite run time. We typically run our simulation for a total time of $\tau_{\text{sim}} \sim 100\langle n_T \rangle$ such that varying τ_{sim} does not measurably change the statistics of n_T . A more systematic way to identify caging would be to explicitly inspect the local obstacle configuration around the walker. However, implementing such a geometric check in our simulations is computationally expensive, and we do not pursue it here. Instead, we infer caging from the behavior of $\Omega(n)$.

Let us denote the whole trajectory by $\{x(1), x(2), x(3), \dots, x(\tau_{\text{sim}})\}$ and the number of distinct visited sites by $\{\Omega(1), \Omega(2), \Omega(3), \dots, \Omega(\tau_{\text{sim}})\}$. Note that by definition $\Omega(n) = \Omega_{\text{sat}}$ for $n \geq n_T$. In our simulation, we look at the quantity $[\Omega_{\text{sat}} - \Omega(n)]$ which is positive for $n < n_T$ and zero for $n \geq n_T$. The first time it becomes zero is the trapping time n_T . Next we repeat this procedure for around $10^3\text{--}10^4$ realizations (depending on ρ) and then take the ensemble average to obtain mean $\langle n_T \rangle$.

We are also interested in the trap size A_T which refers to the number of vacant sites in the trap. For this, we take the part of trajectory from $n_T \leq n \leq \tau_{\text{sim}}$ and count the number of new sites visited using this part. The saturated value of this number represents the trap size A_T for this realization. We then repeat this for other realizations also and obtain the mean $\langle A_T \rangle$.

Finally, in order to calculate the survival probability of not being trapped, we take

$$\begin{aligned} S(n) &= 1, & \text{if } n < n_T, \\ &= 0, & \text{if } n \geq n_T, \end{aligned}$$

and then repeat the same analysis for $10^5\text{--}10^6$ realizations and yield the averaged survival probability.

Appendix B: First-passage visit to $-L_1$ without hitting L_2 for one-dimensional random walk

In this appendix, we consider a random walker moving inside a finite interval $[-L_1, L_2]$ and initially located at the origin. At each time step, it moves symmetrically with probability of $1/2$ to either of its neighboring sites. We are interested in calculating the first-passage probability $\mathcal{F}_1(m|x_0 = 0, \{x_j\}_{j=1}^{m-1} < L_2)$ to $-L_1$ given that the walker has not touched L_2 at intermediate times, *i.e.*, x_1, x_2, \dots, x_{m-1} are all smaller than L_2 . To derive this, we first consider the propagator $\mathcal{P}_{\text{aa}}(x, n|0)$ of finding the walker at some position x inside the interval $[-L_1, L_2]$ after a time step n , with absorbing boundary conditions at $x = -L_1$ and $x = L_2$. The propagator is governed by the

evolution equation

$$\mathcal{P}_{\text{aa}}(x, n+1|0) = \frac{1}{2} \mathcal{P}_{\text{aa}}(x+1, n|0) + \frac{1}{2} \mathcal{P}_{\text{aa}}(x-1, n|0), \quad (\text{B1})$$

with the absorbing boundary conditions

$$\mathcal{P}_{\text{aa}}(-L_1, n|0) = 0, \quad \mathcal{P}_{\text{aa}}(L_2, n|0) = 0. \quad (\text{B2})$$

Our first-passage probability is related to this propagator by [25]

$$\mathcal{F}_1(m|x_0 = 0, \{x_j\}_{j=1}^{m-1} < L_2) = \begin{cases} \frac{1}{2} \mathcal{P}_{\text{aa}}(-L_1 + 1, m-1), & \text{for } L_1 \neq 0, \\ \delta_{m,0}, & \text{for } L_1 = 0, \end{cases} \quad (\text{B3})$$

Since the walker starts from the origin, the first-passage time to $L_1 = 0$ is simply zero. This corresponds to the second relation in Eq. (B3). On the other hand, for any non-zero value of L_1 , the walker must reach $x = -L_1 + 1$ at the $(m-1)$ -th time step and then make a successful jump to $x = -L_1$ with probability 1/2 at the m -th step. This gives rise to the first relation in Eq. (B3). Our goal now is to solve Eq. (B1) with appropriate boundary conditions and then use Eq. (B3) to calculate the first-passage probability.

Given the nature of the boundary conditions, we expand $\mathcal{P}_{\text{aa}}(x, n|0)$ as

$$\mathcal{P}_{\text{aa}}(x, n|0) = \sum_{\theta=1}^L \sin\left[\frac{\pi\theta(x+L_1)}{L}\right] \bar{\mathcal{P}}_{\text{aa}}(\theta, n|0), \quad (\text{B4})$$

with $L = (L_1 + L_2)$. The inverse transformation can be written as

$$\bar{\mathcal{P}}_{\text{aa}}(\theta, n|0) = \frac{2}{L} \sum_{x=-L_1}^{L_2} \sin\left[\frac{\pi\theta(x+L_1)}{L}\right] \mathcal{P}_{\text{aa}}(x, n|0). \quad (\text{B5})$$

To arrive at this inverse transformation, we have used the following property

$$\sum_{x=-L_1}^{L_2} \sin\left[\frac{\pi\theta_1(x+L_1)}{L}\right] \sin\left[\frac{\pi\theta_2(x+L_1)}{L}\right] = \frac{L}{2} \delta_{\theta_1, \theta_2}. \quad (\text{B6})$$

Substituting Eq. (B4) in Eq. (B1) yields the recurrence relation

$$\bar{\mathcal{P}}_{\text{aa}}(\theta, n+1|0) = \cos\left(\frac{\pi\theta}{L}\right) \bar{\mathcal{P}}_{\text{aa}}(\theta, n|0), \quad (\text{B7})$$

which can be solved as

$$\bar{\mathcal{P}}_{\text{aa}}(\theta, n|0) = \cos^n\left(\frac{\pi\theta}{L}\right) \bar{\mathcal{P}}_{\text{aa}}(\theta, 0|0). \quad (\text{B8})$$

We now need the initial value $\bar{\mathcal{P}}_{\text{aa}}(\theta, 0|0)$. For this, we use the initial condition $\mathcal{P}_{\text{aa}}(x, 0|0) = \delta_{x,0}$ in Eq. (B5) and obtain

$$\bar{\mathcal{P}}_{\text{aa}}(\theta, 0|0) = \frac{2}{L} \sin\left(\frac{\pi\theta L_1}{L}\right). \quad (\text{B9})$$

Plugging this in Eq. (B8) completely specifies $\bar{\mathcal{P}}_{\text{aa}}(\theta, n|0)$. The final form of the propagator can now be obtained by using the inverse transformation in Eq. (B5)

$$\mathcal{P}_{\text{aa}}(x, n|0) = \frac{2}{L} \sum_{\theta=1}^L \cos^n\left(\frac{\pi\theta}{L}\right) \sin\left(\frac{\pi\theta L_1}{L}\right) \times \sin\left[\frac{\pi\theta(x+L_1)}{L}\right]. \quad (\text{B10})$$

Having obtained the propagator, we now turn to Eq. (B3) and write the first-passage probability as

$$\mathcal{F}_1(m|x_0 = 0, \{x_j\}_{j=1}^{m-1} < L_2) = \frac{\Theta(m) \Theta(L_1)}{L} \times \sum_{\theta=1}^L \cos^{m-1}\left(\frac{\pi\theta}{L}\right) \sin\left(\frac{\pi\theta L_1}{L}\right) \sin\left(\frac{\pi\theta}{L}\right) + \delta_{L_1, 0} \delta_{m, 0}. \quad (\text{B11})$$

This expression has been quoted in the main text. In addition to this, the propagator $\mathcal{P}_{\text{aa}}(x, n|0)$ can also be employed to evaluate the other first-passage probability $\mathcal{F}_2(m|x_0 = 0, \{x_j\}_{j=1}^{m-1} > -L_1)$ to L_2 given that the walker has not hit $-L_1$

$$\mathcal{F}_2(m|x_0 = 0, \{x_j\}_{j=1}^{m-1} > -L_1) = \begin{cases} \frac{1}{2} \mathcal{P}_{\text{aa}}(L_2 - 1, m-1), & \text{for } L_2 \neq 0, \\ \delta_{m,0}, & \text{for } L_2 = 0. \end{cases} \quad (\text{B12})$$

Utilizing the expression of $\mathcal{P}_{\text{aa}}(x, n|0)$ in Eq. (B10) gives us

$$\mathcal{F}_2(m|x_0 = 0, \{x_j\}_{j=1}^{m-1} > -L_1) = \frac{\Theta(m) \Theta(L_2)}{L} \times \sum_{\theta=1}^L \cos^{m-1}\left(\frac{\pi\theta}{L}\right) \sin\left(\frac{\pi\theta L_2}{L}\right) \sin\left(\frac{\pi\theta}{L}\right) + \delta_{L_2, 0} \delta_{m, 0}.$$

1. Normalization of $\mathcal{F}_1(m|x_0 = 0, \{x_j\}_{j=1}^{m-1} < L_2)$

Due to the presence of an absorbing boundary at $x_{\text{abs}} = L_2$, the probability $\mathcal{F}_1(m|x_0 = 0, \{x_j\}_{j=1}^{m-1} < L_2)$ is not normalised to unity. Rather in the first line of Eq. (15), we saw that

$$\sum_{m=0}^{\infty} \mathcal{F}_1(m|x_0 = 0, \{x_j\}_{j=1}^{m-1} < L_2) = \frac{L_2}{L}. \quad (\text{B13})$$

In the remaining part of this appendix, we will explicitly prove this normalisation. Following Eq. (12), we can write

$$\sum_{m=0}^{\infty} \mathcal{F}_1(m|x_0=0, \{x_j\}_{j=1}^{m-1} < L_2) = \delta_{L_1,0} + \Theta(L_1)\mathcal{J}(L, L_1), \quad (\text{B14})$$

where the function $\mathcal{J}(L, L_1)$ is defined as

$$\mathcal{J}(L, L_1) = \frac{1}{L} \sum_{\theta=1}^L \cot\left(\frac{\pi\theta}{2L}\right) \sin\left(\frac{\pi\theta L_1}{L}\right). \quad (\text{B15})$$

One can rewrite this expression as

$$\begin{aligned} \mathcal{J}(L, L_1) &= \frac{1}{L} \sum_{\theta=1}^{2L-1} \cot\left(\frac{\pi\theta}{2L}\right) \sin\left(\frac{\pi\theta L_1}{L}\right) \\ &\quad - \frac{1}{L} \sum_{\theta=L+1}^{2L-1} \cot\left(\frac{\pi\theta}{2L}\right) \sin\left(\frac{\pi\theta L_1}{L}\right). \end{aligned} \quad (\text{B16})$$

Replacing $\theta \rightarrow (2L - \theta)$ in the second summation, we observe that it becomes identical to $\mathcal{J}(L, L_1)$ and Eq. (B16) reduces to

$$\mathcal{J}(L, L_1) = \frac{1}{2L} \sum_{\theta=1}^{2L-1} \cot\left(\frac{\pi\theta}{2L}\right) \sin\left(\frac{\pi\theta L_1}{L}\right). \quad (\text{B17})$$

Finally, we use the following summation formula [35]

$$\sum_{j=1}^{\alpha_1-1} \cot\left(\frac{\pi j}{\alpha_1}\right) \sin\left(\frac{2\pi j \alpha_2}{\alpha_1}\right) = \alpha_1 - 2\alpha_2, \text{ for } \alpha_2 < \alpha_1. \quad (\text{B18})$$

and simplify Eq. (B17) to

$$\mathcal{J}(L, L_1) = \frac{L_2}{L}. \quad (\text{B19})$$

Inserting this form of $\mathcal{J}(L, L_1)$ in Eq. (B14), we recover the normalisation of $\mathcal{F}_1(m|x_0=0, \{x_j\}_{j=1}^{m-1} < L_2)$ quoted in Eq. (B13). Proceeding in the similar manner, one can find

$$\sum_{m=0}^{\infty} \mathcal{F}_2(m|x_0=0, \{x_j\}_{j=1}^{m-1} > -L_1) = \frac{L_1}{L}. \quad (\text{B20})$$

Appendix C: First-passage probability for a 1d random walker with a reflecting boundary

This section will present a detailed derivation of the first-passage probability $\mathcal{F}_2(m|x_0 = -L_1)$ for reaching L_2 from an initial position $x_0 = -L_1$, in the presence of a reflecting boundary at $x_{\text{ref}} = -L_1$. To this end, we first look at the propagator $\mathcal{P}_{\text{ra}}(x, n|x_0)$ of finding the

walker at some position x (with $-L_1 \leq x \leq L_2$) after n -th time step. The subscript ‘ra’ denotes that the propagator obeys a reflecting boundary condition at $x = -L_1$ and an absorbing boundary condition at $x = L_2$. It satisfies the evolution equation

$$\mathcal{P}_{\text{ra}}(x, n+1|x_0) = \frac{1}{2}\mathcal{P}_{\text{ra}}(x+1, n|x_0) + \frac{1}{2}\mathcal{P}_{\text{ra}}(x-1, n|x_0), \quad (\text{C1})$$

with the boundary conditions

$$\mathcal{P}_{\text{ra}}(-L_1, n) = \mathcal{P}_{\text{ra}}(-L_1 - 1, n), \quad \mathcal{P}_{\text{ra}}(L_2, n) = 0. \quad (\text{C2})$$

Consistent with the absorbing boundary condition, we consider the solution

$$\mathcal{P}_{\text{ra}}(x, n|x_0) = \sin(\pi\omega(L_2 - x)) \bar{\mathcal{P}}_{\text{ra}}(\omega, n|x_0). \quad (\text{C3})$$

The reflecting boundary condition then gives

$$\omega = \frac{(2\theta + 1)}{2(L + \frac{1}{2})}, \quad \text{with } \theta = 0, 1, 2, \dots, L, \quad (\text{C4})$$

where $L = (L_1 + L_2)$. Plugging this in Eq. (C4) yields

$$\mathcal{P}_{\text{ra}}(x, n|x_0) = \sum_{\theta=0}^L \sin\left[\frac{\pi(2\theta + 1)(L_2 - x)}{2(L + \frac{1}{2})}\right] \bar{\mathcal{P}}_{\text{ra}}(\theta, n|x_0). \quad (\text{C5})$$

The inverse transformation can be obtained using Eq. (B6)

$$\begin{aligned} \bar{\mathcal{P}}_{\text{ra}}(\theta, n|x_0) &= \frac{2}{(L + \frac{1}{2})} \sum_{x=-L_1}^{L_2} \sin\left[\frac{\pi(2\theta + 1)(L_2 - x)}{2(L + \frac{1}{2})}\right] \\ &\quad \times \mathcal{P}_{\text{ra}}(x, n|x_0). \end{aligned} \quad (\text{C6})$$

One can solve Eq. (C1) to obtain

$$\bar{\mathcal{P}}_{\text{ra}}(\theta, n|x_0) = \cos^n\left[\frac{\pi(2\theta + 1)}{2(L + \frac{1}{2})}\right] \bar{\mathcal{P}}_{\text{ra}}(\theta, 0|x_0). \quad (\text{C7})$$

To get the unknown $\bar{\mathcal{P}}_{\text{ra}}(\theta, 0|x_0)$, we utilize the initial condition $\mathcal{P}_{\text{ra}}(x, 0|x_0) = \delta_{x, x_0}$ and yield

$$\bar{\mathcal{P}}_{\text{ra}}(\theta, 0|x_0) = \frac{2}{(L + \frac{1}{2})} \sin\left[\frac{\pi(2\theta + 1)(L_2 - x_0)}{2(L + \frac{1}{2})}\right]. \quad (\text{C8})$$

Substituting this in Eq. (C5) gives the propagator

$$\begin{aligned} \mathcal{P}_{\text{ra}}(x, n|x_0) &= \frac{2}{(L + \frac{1}{2})} \sum_{\theta=0}^L \cos^n\left[\frac{\pi(2\theta + 1)}{2(L + \frac{1}{2})}\right] \\ &\quad \times \sin\left[\frac{\pi(2\theta + 1)(L_2 - x)}{2(L + \frac{1}{2})}\right] \sin\left[\frac{\pi(2\theta + 1)(L_2 - x_0)}{2(L + \frac{1}{2})}\right], \end{aligned} \quad (\text{C9})$$

which for $x_0 = -L_1$ reduces to

$$\begin{aligned} \mathcal{P}_{\text{ra}}(x, n| -L_1) &= \frac{2}{(L + \frac{1}{2})} \sum_{\theta=0}^L \cos^n \left[\frac{\pi(2\theta + 1)}{2(L + \frac{1}{2})} \right] \\ &\times \cos \left[\frac{\pi(2\theta + 1)}{4(L + \frac{1}{2})} \right] \cos \left[\frac{\pi(x + L_1 + \frac{1}{2})(2\theta + 1)}{2(L + \frac{1}{2})} \right]. \end{aligned} \quad (\text{C10})$$

With the propagator now at hand, we proceed to compute the first-passage probability as follows [25]

$$\mathcal{F}_2(m|x_0 = -L_1) = \frac{1}{2} \mathcal{P}_{\text{ra}}(L_2 - 1, m - 1| -L_1). \quad (\text{C11})$$

As explained in Appendix B, this relation is based on the fact that the walker can reach L_2 at the m -th step only if it was at $L_2 - 1$ at the $(m - 1)$ time step and then made a successful jump to $x = L_2$ with probability 1/2. Employing the expression of propagator derived above, we find

$$\begin{aligned} \mathcal{F}_2(m|x_0 = -L_1) &= \sum_{\theta=0}^L (-1)^\theta \cos^{m-1} \left(\frac{\pi(2\theta + 1)}{2(L + \frac{1}{2})} \right) \\ &\times \cos \left(\frac{\pi(2\theta + 1)}{4(L + \frac{1}{2})} \right) \sin \left(\frac{\pi(2\theta + 1)}{2(L + \frac{1}{2})} \right) \frac{\Theta(m)\Theta(L)}{(L + \frac{1}{2})}. \end{aligned} \quad (\text{C12})$$

By symmetry, we have $\mathcal{F}_2(m|x_0 = -L_1) = \mathcal{F}_1(m|x_0 = L_2)$ and the same expression holds for $\mathcal{F}_1(m|x_0 = L_2)$ as well. Moreover, it is derived under the assumption of the reflecting boundary condition. Consequently it should be correctly normalised to unity

$$\sum_{m=0}^{\infty} \mathcal{F}_2(m|x_0 = -L_1) = \sum_{m=0}^{\infty} \mathcal{F}_1(m|x_0 = L_2) = 1. \quad (\text{C13})$$

Appendix D: Survival probability $Q(n|L_1, L_2)$ for large n

In the large- n limit, we saw that the survival probability $Q(n|L_1, L_2)$ for fixed L_1 and L_2 decays exponentially with time, see Eq. (18). In order to prove this, we first note that for the walker to survive for a long duration, the interval $[-L_1, L_2]$ over which it moves also has to be large. In the asymptotic regime where both n and L are large while keeping the ratio n/L^2 finite, we find that the first-passage probabilities appearing in Eqs. (12)-(14) satisfy the scaling relation

$$\begin{aligned} \mathcal{F}_1 \left(n|x_0 = 0, \{x_j\}_{j=1}^{m-1} < L_2 \right) &\simeq g_1(n/L^2), \\ \mathcal{F}_2 \left(n|x_0 = 0, \{x_j\}_{j=1}^{m-1} > -L_1 \right) &\simeq g_2(n/L^2), \\ \mathcal{F}_1(n|x_0 = L_2) &\simeq g_3(n/L^2), \end{aligned} \quad (\text{D1})$$

with the g -functions defined as

$$g_1(z) = \frac{\pi}{L^2} \sum_{\theta=1}^{\infty} \theta \sin \left(\frac{\pi\theta L_1}{L} \right) \exp \left(-\frac{z\pi^2\theta^2}{2} \right), \quad (\text{D2})$$

$$g_2(z) = \frac{\pi}{L^2} \sum_{\theta=1}^{\infty} \theta \sin \left(\frac{\pi\theta L_2}{L} \right) \exp \left(-\frac{z\pi^2\theta^2}{2} \right), \quad (\text{D3})$$

$$g_3(z) = \frac{\pi}{L^2} \sum_{\theta=0}^{\infty} (-1)^\theta \frac{(2\theta + 1)}{2} \exp \left(-\frac{z\pi^2(2\theta + 1)^2}{8} \right). \quad (\text{D4})$$

Plugging Eq. (D1) in Eq. (11), we obtain

$$\begin{aligned} P(n_T|L_1, L_2) &\simeq \Theta(L) \sum_{m=0}^{n_T} [g_1(m/L^2) + g_2(m/L^2)] \\ &\times g_3((n_T - m)/L^2). \end{aligned} \quad (\text{D5})$$

We perform the variable transformation $\kappa = m/L^2$ and for large L , we can treat κ as a continuous variable to rewrite Eq. (D5) as

$$P(\omega|L_1, L_2) \simeq \Theta(L) \int_0^\omega d\kappa [g_1(\kappa) + g_2(\kappa)] g_3(\omega - \kappa), \quad (\text{D6})$$

where $\omega = n_T/L^2$. Taking Laplace transformation with respect to $\omega \rightarrow s$ and using the convolution structure of the right-hand side, we obtain

$$\bar{P}(s|L_1, L_2) \simeq \Theta(L) [\bar{g}_1(s) + \bar{g}_2(s)] \bar{g}_3(s), \quad (\text{D7})$$

where $\bar{P}(s|L_1, L_2)$ stands for the Laplace transform of $P(\omega|L_1, L_2)$ and similarly for the g -functions. Following Eqs. (D2)-(D4), we have

$$\begin{aligned} \bar{g}_1(s) &= \frac{\sinh(\sqrt{2s}L_2)}{\sinh(\sqrt{2s}L)}, \quad \bar{g}_2(s) = \frac{\sinh(\sqrt{2s}L_1)}{\sinh(\sqrt{2s}L)}, \\ \bar{g}_3(s) &= \frac{1}{\cosh(\sqrt{2s}L)}, \end{aligned} \quad (\text{D8})$$

and inserting them in Eq. (D7) yields

$$\begin{aligned} \bar{P}(s|L_1, L_2) &\simeq 2\Theta(L) \operatorname{csch} \left(2\sqrt{2s}L \right) \\ &\times [\sinh(\sqrt{2s}L_1) + \sinh(\sqrt{2s}L_2)]. \end{aligned} \quad (\text{D9})$$

This gives us the trapping time probability in the Laplace domain when both L_1 and L_2 are large. One can use it to obtain various moments of n_T . For example, the mean $\langle n_T \rangle$ can be found to be

$$\langle n_T | L_1, L_2 \rangle = L_1^2 + L_2^2 + 3L_1L_2. \quad (\text{D10})$$

In fact, one can perform the inverse Laplace transform of Eq. (D9) and get the full distribution

$$\begin{aligned} P(n_T|L_1, L_2) &= \frac{\pi}{2L^2} \sum_{\theta} (-1)^{\theta-1} \theta \left[\sin \left(\frac{\pi\theta L_1}{2L} \right) \right. \\ &\left. + \sin \left(\frac{\pi\theta L_2}{2L} \right) \right] \exp \left(-\frac{\theta^2\pi^2 n_T}{8L^2} \right) \Theta(L), \end{aligned} \quad (\text{D11})$$

where recall that $\omega = n_T/L^2$. From this, the survival probability that the particle has not been trapped follows to be

$$\begin{aligned} Q(n|L_1, L_2) &\simeq L^2 \int_{n/L^2}^{\infty} d\kappa P(n_T = \kappa L^2|L_1, L_2), \\ &\simeq \frac{4}{\pi} \sum_{\theta=1}^{\infty} \frac{(-1)^{\theta-1}}{\theta} \left[\sin\left(\frac{\pi\theta L_1}{2L}\right) + \sin\left(\frac{\pi\theta L_2}{2L}\right) \right] \\ &\quad \times \exp\left(-\frac{\theta^2\pi^2 n}{8L^2}\right) \Theta(L). \end{aligned} \quad (\text{D12})$$

Then, the leading order decay of the survival probability $n/L^2 \gg 1$ reads as

$$\begin{aligned} Q(n|L_1, L_2) &\simeq \frac{4}{\pi} \left[\sin\left(\frac{\pi L_1}{2L}\right) + \sin\left(\frac{\pi L_2}{2L}\right) \right] \\ &\quad \times \exp\left(-\frac{\pi^2 n}{8L^2}\right) \Theta(L). \end{aligned} \quad (\text{D13})$$

1. Survival probability for the Sokoban walker with $N_P = 1$

We next compute the average of $Q(n|L_1, L_2)$ for the Sokoban model using the joint probability of $q(L, L_i|N_P = 1)$ with $i \in \{1, 2\}$. As seen before in Eq. (30), the joint probability for $N_P = 1$ can be calculated as

$$\begin{aligned} q(L, L_i|N_P = 1) &= \rho^4 (L_i + 1) (L - L_i + 1) (1 - \rho)^L \\ &\quad \times \Theta(L - L_i). \end{aligned} \quad (\text{D14})$$

The survival probability is given

$$\begin{aligned} S(n|N_P = 1) &\simeq \frac{4}{\pi} \sum_{L=1}^{\infty} \sum_{i=1}^2 \sum_{L_i=1}^L q(L, L_i|N_P = 1) \\ &\quad \times \sin\left(\frac{\pi L_i}{2L}\right) \exp\left(-\frac{\pi^2 n}{8L^2}\right), \\ &\simeq \frac{8\rho^4}{\pi} \sum_{L=1}^{\infty} \mathcal{H}(L) (1 - \rho)^L e^{-\frac{\pi^2 n}{8L^2}}. \end{aligned} \quad (\text{D15})$$

with $\mathcal{H}(L)$ defined as

$$\mathcal{H}(L) = \sum_{L_1=1}^L (L_1 + 1) (L - L_1 + 1) \sin\left(\frac{\pi L_1}{2L}\right), \quad (\text{D16})$$

$$\begin{aligned} &= \frac{1}{4} \left[2 + L + \cot\left(\frac{\pi}{4L}\right) \left\{ 3 + 2L - L \cot\left(\frac{\pi}{4L}\right) \right. \right. \\ &\quad \left. \left. + \cot^2\left(\frac{\pi}{4L}\right) \right\} \right], \end{aligned} \quad (\text{D17})$$

$$\begin{aligned} &\simeq \frac{4(4 - \pi)L^3}{\pi^3} + \frac{2L^2}{\pi} + \frac{(24 + 5\pi)L}{12\pi} + \frac{(12 - \pi)}{24}, \\ &\quad \text{for } L \gg 1. \end{aligned} \quad (\text{D18})$$

In the last expression, we have also written down the large- L behavior of $\mathcal{H}(L)$ for later use. Turning

to Eq. (D15), we perform a change of variable $u = 2\sqrt{2L}/\pi\sqrt{n}$ and change the summation into an integral for large n

$$S(n|N_P = 1) \simeq 2\sqrt{2n}\rho^4 \int_0^{\infty} du \mathcal{H}\left(\frac{2\alpha}{\lambda}u\right) e^{-\frac{1}{u^2} - 2\alpha u}, \quad (\text{D19})$$

$$\text{where } \alpha = \frac{\lambda\pi\sqrt{n}}{4\sqrt{2}}, \quad \lambda = |\ln(1 - \rho)|. \quad (\text{D20})$$

For $n \gg 1$, one also has $\alpha \gg 1$ and this enables us to use the asymptotic expression for \mathcal{H} -function from Eq. (D18). The survival probability then turns out to be

$$\begin{aligned} S(n|N_P = 1) &\simeq 2\sqrt{2n}\rho^4 \int_0^{\infty} du \left[\frac{32\alpha^3(4 - \pi)}{\pi^3\lambda^3} u^3 + \frac{8\alpha^2}{\pi\lambda^2} u^2 \right. \\ &\quad \left. \frac{\alpha(24 + 5\pi)}{6\pi\lambda} u + \frac{(12 - \pi)}{24} \right] e^{-\frac{1}{u^2} - 2\alpha u}. \end{aligned} \quad (\text{D21})$$

As illustrated in Eq. (34), the integration over u can be carried out in terms of Meijer-G function. After this, Eq. (D21) becomes

$$S(n|N_P = 1) \simeq \left[\frac{32(4 - \pi)}{\pi^3\lambda^3} G_{0\ 3}^{3\ 0} \left(0, \frac{-}{2, \frac{5}{2}} \middle| \alpha^2 \right) + \frac{8}{\pi\lambda^2} G_{0\ 3}^{3\ 0} \left(0, \frac{-}{2, 2} \middle| \alpha^2 \right) + \right. \\ \left. \frac{(24 + 5\pi)}{6\pi\lambda} G_{0\ 3}^{3\ 0} \left(0, \frac{-}{1, \frac{3}{2}} \middle| \alpha^2 \right) + \frac{(12 - \pi)}{24} G_{0\ 3}^{3\ 0} \left(0, \frac{-}{\frac{1}{2}, 1} \middle| \alpha^2 \right) \right] \frac{8\rho^4}{\lambda\pi^{\frac{3}{2}}}.$$

By noting that α depends on n through Eq. (D20), one can further simplify this expression by employing the asymptotic form of the G-functions using *Mathematica*

$$G_{0\ 3}^{3\ 0} \left(0, \frac{-}{1, \frac{1+m}{2}, \frac{2+m}{2}} \middle| \alpha^2 \right) \simeq e^{-3\alpha^{\frac{2}{3}}} \left[\mathbb{R}_m(\alpha) + \mathcal{O}\left(\frac{1}{\alpha^{\frac{1}{3}}}\right) \right], \quad (\text{D22})$$

where

$$\mathbb{R}_0(\alpha) = \frac{2\pi}{\sqrt{3}}\alpha^{\frac{1}{3}}, \quad (\text{D23})$$

$$\mathbb{R}_1(\alpha) = \frac{2\pi}{\sqrt{3}}\alpha + \frac{17\pi}{18\sqrt{3}}\alpha^{\frac{1}{3}}, \quad (\text{D24})$$

$$\mathbb{R}_2(\alpha) = \frac{2\pi}{\sqrt{3}}\alpha^{\frac{5}{3}} + \frac{35\pi}{18\sqrt{3}}\alpha + \frac{1225\pi}{1296\sqrt{3}}\alpha^{\frac{1}{3}}, \quad (\text{D25})$$

$$\mathbb{R}_3(\alpha) = \frac{2\pi}{\sqrt{3}}\alpha^{\frac{7}{3}} + \frac{59\pi}{18\sqrt{3}}\alpha^{\frac{5}{3}} + \frac{3745\pi}{1296\sqrt{3}}\alpha + \frac{199115\pi}{139968\sqrt{3}}\alpha^{\frac{1}{3}}. \quad (\text{D26})$$

With these asymptotic forms, the long-time behavior of the survival probability simplifies to

$$S(n|N_P = 1) \simeq \mathcal{K}_1(n) \exp\left(-\frac{3\pi^{2/3}}{2^{5/3}}\lambda^{2/3}n^{1/3}\right), \quad (\text{D27})$$

where the prefactor $\mathcal{K}_1(n)$ reads as

$$\begin{aligned} \mathcal{K}_1(n) &= \frac{8\rho^4}{\lambda\pi^{3/2}} \left[\frac{32(4-\pi)}{\pi^3\lambda^3} \mathbb{R}_3(\alpha) + \frac{8}{\pi\lambda^2} \mathbb{R}_2(\alpha) \right. \\ &\quad \left. + \frac{(24+5\pi)}{6\pi\lambda} \mathbb{R}_1(\alpha) + \frac{(12-\pi)}{24} \mathbb{R}_0(\alpha) \right], \quad (\text{D28}) \end{aligned}$$

$$\simeq \frac{2^{\frac{19}{6}}(4-\pi)\rho^4}{\sqrt{3}\pi^{\frac{7}{6}}\lambda^{\frac{5}{3}}} n^{\frac{7}{6}}, \quad \text{for } n \gg 1. \quad (\text{D29})$$

2. Survival probability at intermediate times

The survival probability $Q(n|L_1, L_2)$ given in Eq. (D13) works only for $n/L^2 \gg 1$. For small values of n/L^2 , one needs to retain all terms in Eq. (D12). In this section, we show that it is possible to derive another expression for the survival probability which works well when the rescaled variable $n/L^2 \ll 1$. Our starting point is to rewrite the Laplace transform in Eq. (D9) as

$$\begin{aligned} \bar{P}(s|L_1, L_2) &\simeq \sum_{m=0}^{\infty} \left[\exp\left(-\sqrt{2s}[-(4m+1)L_1 + (4m+2)L_2]\right) \right. \\ &\quad + \exp\left(-\sqrt{2s}[-(4m+2)L_1 + (4m+1)L_2]\right) \\ &\quad - \exp\left(-\sqrt{2s}[-(4m+3)L_1 + (4m+2)L_2]\right) \\ &\quad \left. - \exp\left(-\sqrt{2s}[-(4m+2)L_1 + (4m+3)L_2]\right) \right] 2\Theta(L). \quad (\text{D30}) \end{aligned}$$

Our goal is to analyze this expression for $sL^2 \gg 1$ (equivalently $n/L^2 \ll 1$). In this limit, the leading order contribution to $\bar{P}(s|L_1, L_2)$ will come from $m = 0$ term in the first line of Eq. (D30)

$$\bar{P}(s|L_1, L_2) = 2\Theta(L) \left[e^{-\sqrt{2s}(L_1+2L_2)} + e^{-\sqrt{2s}(2L_1+L_2)} \right]. \quad (\text{D31})$$

Performing the inverse Laplace transformation

$$\begin{aligned} P(n_T|L_1, L_2) &\simeq \sqrt{\frac{2}{\pi n_T^3}} \left[(L_1 + 2L_2) e^{-\frac{(L_1+2L_2)^2}{2n_T}} \right. \\ &\quad \left. + (L_1 + 2L_2) e^{-\frac{(2L_1+L_2)^2}{2n_T}} \right] \Theta(L), \quad (\text{D32}) \end{aligned}$$

which then gives the survival probability

$$\begin{aligned} Q(n|L_1, L_2) &= 1 - \int_0^n dn_T P(n_T|L_1, L_2), \\ &\simeq 1 - 2 \left[\text{erfc}\left(\frac{L_1+2L_2}{\sqrt{2n}}\right) + \text{erfc}\left(\frac{2L_1+L_2}{\sqrt{2n}}\right) \right] \Theta(L), \quad (\text{D33}) \end{aligned}$$

for $n/L^2 \ll 1$. We now have to average over L_1 and L_2 . For small densities

$$q(L_i|N_P=0) \simeq \rho e^{-\rho L_i}, \quad q(L_i|N_P=1) \simeq \rho^2 L_i e^{-\rho L_i}, \quad (\text{D34})$$

where $i \in \{1, 2\}$. With this at hand, we get

$$\begin{aligned} S(n|N_P=0) &\simeq 1 - \rho^2 \int_0^n dn_T \sum_{L_1, L_2=1}^{\infty} e^{-\rho(L_1+L_2)} \\ &\quad \times P(n_T|L_1, L_2). \quad (\text{D35}) \end{aligned}$$

This expression can be simplified to

$$\begin{aligned} S(n|N_P=0) &\simeq 1 - \frac{2\sqrt{2}\rho^2}{\sqrt{\pi}} \int_0^n dn_T 2^{3/2} \int_0^{\infty} dw_1 \\ &\quad \times \int_0^{\infty} dw_2 (w_1 + 2w_2) e^{-(w_1+2w_2)^2}. \quad (\text{D36}) \end{aligned}$$

Upon carrying out the integrations over w_1 and w_2 , we obtain

$$S(n|N_P=0) \simeq 1 - n\rho^2. \quad (\text{D37})$$

Proceeding in a similar manner for $N_P = 1$ yields

$$S(n|N_P=1) \simeq 1 - \frac{n^2\rho^4}{8}. \quad (\text{D38})$$

Appendix E: Divergence of $\langle n_T \rangle$ and $\langle A_T \rangle$ for the AIL model

In Figs. 10 and 11, we demonstrated that the mean trapping time and mean trap size exhibits a monotonic dependence on ρ for the two-dimensional AIL model, with both averages diverging at the percolation threshold, $\rho \rightarrow \rho_c^+$, where $\rho_c \approx 0.407$. The divergence can be heuristically understood through the formation of giant clusters of vacant sites. When ρ is close to unity, the lattice is almost completely occupied by the obstacles, with only small, sparsely distributed clusters of vacant sites. Consequently, the caging effect is quite strong in this regime and the motion of the walker is strongly inhibited. When ρ is decreased, these clusters start to merge together and below the critical density, $\rho \leq \rho_c$, a giant cluster of infinite size emerges. In some realizations, the AIL walker can be present in such a giant cluster of vacant sites. Under this situation, the number of distinct sites to be visited is infinite, and the time required to explore them all also diverges. This results in the divergence of $\langle n_T \rangle$ and $\langle A_T \rangle$ at and below the percolation threshold.

When ρ is slightly above, but close to, the threshold ρ_c , a large cluster of vacancies can still be present, but its size is finite. The typical lengthscale of the clusters $\xi(\rho)$ scales with the density as [3]

$$\xi(\rho) \sim 1/(\rho - \rho_c)^{4/3}, \quad \text{for } \rho \gtrsim \rho_c. \quad (\text{E1})$$

Consider now the AIL walker moving in this large but finite cluster of vacant sites. It gets trapped when it has visited all the vacant sites in this cluster. If we focus on smaller time scales, $n \ll n_T$, then the walker does

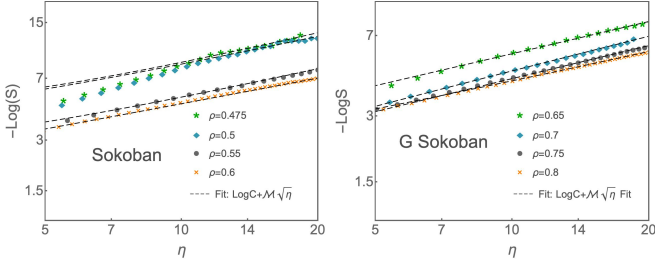


FIG. 15. Plot of $\log S(\eta)$ versus η for the two-dimensional Sokoban and G-Sokoban models in the log-log scale. Each panel shows simulation data for different densities (shown by symbols). The dashed lines represent fits to the data based on the stretched-exponential form in Eq. (F2). The linear trend at large η in the log-log scale reflects the $\sqrt{\eta}$ behavior of $\log S(\eta)$. The slope of each fit yields the decay coefficient $\mathcal{M}_\#(\rho)$, while the vertical offset provides an estimate of the prefactor $C_\#(\eta)$. The estimated values of $\mathcal{M}_\#(\rho)$ are given in Eq. (69), while that of $C_\#(\eta)$ are presented in Table I.

not realise the finiteness of the cluster. The dynamics, then, is effectively like in an infinite cluster where the walker is known to move sub-diffusively and its mean-squared displacement (MSD) behaves as $\langle r_n^2 \rangle \sim n^{2/d_W}$ with the exponent $d_W \approx 2.878$ [3]. On the other hand, at large time scales, $n \gg n_T$, the AIL walker has visited all vacant sites in the cluster and the MSD saturates to $\langle r_n^2 \rangle \sim \xi^2(\rho)$. Rewriting these two limits

$$\langle r_n^2 \rangle \sim \begin{cases} n^{\frac{2}{d_W}}, & \text{for } n \ll n_T, \\ \xi^2(\rho), & \text{for } n \gg n_T, \end{cases} \quad (\text{E2})$$

the saturation takes place at the time scale $n_T \sim \xi^{d_W}(\rho)$. Plugging $\xi(\rho)$ from Eq. (E1), the trapping time should diverge as

$$\langle n_T \rangle \sim 1/(\rho - \rho_c)^{\gamma_{\text{AIL}}}, \quad (\text{E3})$$

with the exponent $\gamma_{\text{AIL}} = 4d_W/3 \approx 3.8373$. This divergence is compared with the numerical simulations in Fig. 10 (right panel).

We next turn to $\langle A_T \rangle$. By our definition, the walker will be trapped if it does not visit any new distinct sites. For an AIL walker moving in a cluster of vacant sites, the trap size is determined by the size of the cluster. As explained before, for $\rho \leq \rho_c$, the average cluster size is infinite which implies that the average trap size $\langle A_T \rangle$ is also infinite. Around the percolation threshold, $\rho \gtrsim \rho_c$, the mean cluster size diverges as $\sim (\rho - \rho_c)^{-43/18}$ [36]. Therefore, we get

$$\langle A_T \rangle \sim (\rho - \rho_c)^{-43/18}, \quad \text{for } \rho \gtrsim \rho_c. \quad (\text{E4})$$

In Fig. 11 (right panel), we compare this divergence of $\langle A_T \rangle$ with the numerical simulations and find a good agreement between simulations and theory.

Model	Density ρ	Prefactor $C_\#(\eta)$
Sokoban	0.475	$\eta^{2.8}$
	0.50	$\eta^{1.55}$
	0.55	$\eta^{1.25}$
	0.60	$\eta^{0.1}$
G-Sokoban	0.65	0.8604
	0.70	1.349
	0.75	1.0
	0.80	0.576

TABLE I. Numerical estimates of the prefactor $C_\#(\eta)$ for different values of the density ρ in each model.

Appendix F: Numerical estimation of $C_\#(\eta)$ and $\mathcal{M}_\#(\rho)$

In this appendix, we will explain how we estimate the quantities $C_\#(\eta)$ and $\mathcal{M}_\#(\rho)$ appearing in Eq. (68), where $\#$ stands for the sok or Gsok depending on the model. These quantities are not known analytically in two dimensions and must therefore be extracted through a fitting procedure. In Fig. 15, we plot $\log S(\eta)$ versus η for both models. Each panel corresponds to one of the two models studied, and within each panel, we show multiple curves corresponding to different values of the density ρ . These plots provide a direct visualization of how the survival probability varies across densities, and form the basis of our fitting procedure.

For a fixed density, the large- η regime exhibits a clear linear trend in the $\log S(\eta)$ versus $\eta^{1/2}$ plot, consistent with the expected stretched-exponential decay

$$S(\eta) \simeq C_\#(\eta) \exp(-\mathcal{M}_\#(\rho) \eta^{1/2}). \quad (\text{F1})$$

Taking the logarithm yields

$$\log S(\eta) \simeq \log C_\#(\eta) - \mathcal{M}_\#(\rho) \eta^{1/2}, \quad (\text{F2})$$

so that $\log S(\eta)$ becomes approximately linear in $\eta^{1/2}$ for sufficiently large η . From the slope of this linear region, we extract $\mathcal{M}_\#(\rho)$, which quantifies the rate of decay and depends on the density. The vertical offset of the fit gives the prefactor $C_\#(\eta)$, which is sub-exponential and varies more slowly with η . By repeating this procedure for different densities, we obtain the decay coefficient $\mathcal{M}_\#(\rho)$, as outlined in Eq. (69). On the other hand, while we do not have an expression for the prefactor $C_\#(\eta)$, its values for considered densities in Fig. 15 are given in Table I.

[1] S. R. Broadbent and J. M. Hammersley, Percolation processes: I. crystals and mazes, *Mathematical Proceedings of the Cambridge Philosophical Society* **53**, 629–641 (1957).
[2] G. H. Weiss, *Aspects and Applications of the Random Walk* (North-Holland, New York, 1994).

[3] D. Ben-Avraham and S. Havlin, *Diffusion and Reactions in Fractals and Disordered Systems* (Cambridge University Press, 2000).

[4] V. Ambegaokar, B. I. Halperin, and J. S. Langer, Hopping conductivity in disordered systems, *Phys. Rev. B* **4**, 2612 (1971).

[5] P. Sheng and J. Klafter, Hopping conductivity in granular disordered systems, *Phys. Rev. B* **27**, 2583 (1983).

[6] M. Sahimi, Flow phenomena in rocks: from continuum models to fractals, percolation, cellular automata, and simulated annealing, *Rev. Mod. Phys.* **65**, 1393 (1993).

[7] E. Barkai, Y. Garini, and R. Metzler, Strange kinetics of single molecules in living cells, *Physics Today* **65**, 29 (2012).

[8] R. Metzler, J.-H. Jeon, A. G. Cherstvy, and E. Barkai, Anomalous diffusion models and their properties: non-stationarity, non-ergodicity, and ageing at the centenary of single particle tracking, *Phys. Chem. Chem. Phys.* **16**, 24128 (2014).

[9] C. Bechinger, R. Di Leonardo, H. Löwen, C. Reichhardt, G. Volpe, and G. Volpe, Active particles in complex and crowded environments, *Rev. Mod. Phys.* **88**, 045006 (2016).

[10] P. Singh, S. Sabhapandit, and A. Kundu, Run-and-tumble particle in inhomogeneous media in one dimension, *Journal of Statistical Mechanics: Theory and Experiment* **2020**, 083207 (2020).

[11] P. G. de Gennes, La percolation: un concept unificateur, *La Recherche* **7**, 919 (1976).

[12] R. M. Ziff and B. Sapoval, The efficient determination of the percolation threshold by a frontier-generating walk in a gradient, *Journal of Physics A: Mathematical and General* **19**, L1169 (1986).

[13] C. D. Lorenz and R. M. Ziff, Precise determination of the bond percolation thresholds and finite-size scaling corrections for the sc, fcc, and bcc lattices, *Phys. Rev. E* **57**, 230 (1998).

[14] O. L. Bonomo and S. Reuveni, Loss of percolation transition in the presence of simple tracer-media interactions, *Phys. Rev. Res.* **5**, L042015 (2023).

[15] O. L. Bonomo, I. Shitrit, and S. Reuveni, Sokoban percolation on the bethe lattice, *Journal of Physics A: Mathematical and Theoretical* **57**, 33LT01 (2024).

[16] Sokoban — wikipedia, <https://en.wikipedia.org/wiki/Sokoban>, retrieved on 11-02-2026.

[17] A. Altshuler, O. L. Bonomo, N. Gorohovsky, S. Marchini, E. Rosen, O. Tal-Friedman, S. Reuveni, and Y. Roichman, Environmental memory facilitates search with home returns, *Phys. Rev. Res.* **6**, 023255 (2024).

[18] A. Biswas, J. M. Cruz, P. Parmananda, and D. Das, First passage of an active particle in the presence of passive crowders, *Soft Matter* **16**, 6138 (2020).

[19] C. S. Dias, M. Trivedi, G. Volpe, N. A. M. Araújo, and G. Volpe, Environmental memory boosts group formation of clueless individuals, *Nature Communications* **14**, 7324 (2023).

[20] P. Singh, D. A. Kessler, and E. Barkai, Sokoban random walk: From environment reshaping to trapping crossover, *Phys. Rev. Res.* **8**, L012023 (2026).

[21] H. B. Rosenstock, Luminescent emission from an organic solid with traps, *Phys. Rev.* **187**, 1166 (1969).

[22] B. Y. Balagurov and V. G. Vaks, Random walks of a particle on lattices with traps, *Journal of Experimental and Theoretical Physics* **38**, 968 (1974).

[23] M. D. Donsker and S. R. S. Varadhan, On the number of distinct sites visited by a random walk, *Communications on Pure and Applied Mathematics* **32**, 721 (1979).

[24] J. K. Anlauf, Asymptotically exact solution of the one-dimensional trapping problem, *Phys. Rev. Lett.* **52**, 1845 (1984).

[25] S. Redner, *A Guide to First-Passage Processes* (Cambridge University Press, 2001).

[26] A. Dvoretzky and P. Erdős, Some problems on random walk in space, in *Proceedings of the Second Berkeley Symposium on Mathematical Statistics and Probability* (University of California Press, Berkeley, 1951) pp. 353–367.

[27] H. Larralde, P. Trunfio, S. Havlin, H. E. Stanley, and G. H. Weiss, Number of distinct sites visited by n random walkers, *Phys. Rev. A* **45**, 7128 (1992).

[28] A. Kundu, S. N. Majumdar, and G. Schehr, Exact distributions of the number of distinct and common sites visited by n independent random walkers, *Phys. Rev. Lett.* **110**, 220602 (2013).

[29] L. C. Andrews, *Special Functions for Engineers and Applied Mathematicians* (New York: Macmillan, 1985).

[30] H. Touchette, The large deviation approach to statistical mechanics, *Physics Reports* **478**, 1 (2009).

[31] H. Touchette, Introduction to dynamical large deviations of markov processes, *Physica A: Statistical Mechanics and its Applications* **504**, 5 (2018), lecture Notes of the 14th International Summer School on Fundamental Problems in Statistical Physics.

[32] I. N. Burenev, D. W. H. Cloete, V. Kharbanda, and H. Touchette, An introduction to large deviations with applications in physics, *SciPost Phys. Lect. Notes* **104** (2025).

[33] R. Borrego, E. Abad, and S. B. Yuste, Survival probability of a subdiffusive particle in a d -dimensional sea of mobile traps, *Phys. Rev. E* **80**, 061121 (2009).

[34] O. L. Bonomo, I. Shitrit, S. Reuveni, and S. Redner, Diffusion/subdiffusion in the pushy random walk, *arXiv:2602.07387* (2025).

[35] M. Beck and M. Halloran, Finite trigonometric character sums via discrete fourier analysis, *International Journal of Number Theory* **06**, 51 (2010).

[36] D. Stauffer and A. Aharony, *Introduction to percolation theory*, 2nd ed. (Taylor & Francis, 1992).